



Research article

Bioinformatics analysis based on extracted ingredients combined with network pharmacology, molecular docking and molecular dynamics simulation to explore the mechanism of Jinbei oral liquid in the therapy of idiopathic pulmonary fibrosis

Xinru Han ^{a,b,1}, Aijun Zhang ^{a,c,1}, Zhaoqing Meng ^c, Qian Wang ^b, Song Liu ^a, Yunjia Wang ^a, Jiaxin Tan ^a, Lubo Guo ^{b,*}, Feng Li ^{a,**}

^a Shandong University of Traditional Chinese Medicine, Jinan, China

^b Department of Pharmacy, Central Hospital Affiliated to Shandong First Medical University, Jinan, China

^c Institute of Chinese Materia Medica, Shandong Hongji-tang Pharmaceutical Group Co., Ltd., Jinan, China

ARTICLE INFO

Keywords:

Jinbei oral liquid
Idiopathic pulmonary fibrosis
Network pharmacology
Molecular docking
Molecular dynamics simulation
Realistic ingredients

ABSTRACT

Objective: Jinbei oral liquid (JBOL), which is derived from a traditional hospital preparation, is frequently utilized to treat idiopathic pulmonary fibrosis (IPF) and has shown efficacy in clinical therapy. However, there are now several obstacles facing the mechanism inquiry, including target proteins, active components, and the binding affinity between crucial compounds and target proteins. To gain additional insight into the mechanisms underlying JBOL in anti-IPF, this study used bioinformatics technologies, including network pharmacology, molecular docking, and molecular dynamic simulation, with a substantial amount of data based on realistic constituents. **Methods:** Using network pharmacology, we loaded 118 realistic compounds into the SwissTargetPrediction and SwissADME databases and screened the active compounds and target proteins. IPF-related targets were collected from the OMIM, DisGeNET, and GeneCards databases, and the network of IPF-active constituents was built with Cytoscape 3.10.1. The GO and KEGG pathway enrichment analyses were carried out using Metascape, and the protein-protein interaction (PPI) network was constructed to screen the key targets with the STRING database. Finally, the reciprocal affinity between the active molecules and the crucial targets was assessed through the use of molecular docking and molecular dynamics simulation.

Results: A total of 122 targets and 34 tested active compounds were summarized in this investigation. Among these, kaempferol, apigenin, baicalein were present in high degree. PPI networks topological analysis identified eight key target proteins. AGE-RAGE, EGFR, and PI3K-Akt signaling pathways were found to be regulated during the phases of cell senescence, inflammatory response, autophagy, and immunological response in anti-IPF of JBOL. It was verified by molecular docking and molecular dynamics simulation that the combining way and binding energy between active ingredients and selected targets.

Conclusions: This work forecasts the prospective core ingredients, targets, and signal pathways of JBOL in anti-IPF, which has confirmed the multiple targets and pathways of JBOL in anti-IPF and

* Corresponding author.

** Corresponding author.

E-mail addresses: 13370582799@163.com (L. Guo), 13969141796@163.com (F. Li).

¹ These two authors contributed equally to this work.

provided the first comprehensive assessment with bioinformatic approaches. With empirical backing and an innovative approach to the molecular mechanism, JBOL is being considered as a potential new medication.

1. Introduction

Idiopathic pulmonary fibrosis (IPF) is a chronic intractable progressive fibrotic interstitial pulmonary disease, characterized by irreversible destruction of the lung parenchyma, excessive extracellular matrix (ECM) deposition, and an aberrant wound healing response brought on by damage to alveolar epithelial cells (AECs) [1]. Due to its uncertain etiology and poorer prognosis—especially with a median survival of 3.8 years (95 % CI 3.5–3.8) [2] since the time of diagnosis in adults aged 65 years or older—it is a serious issue in global public health. End-stage respiratory failure, pulmonary hypertension, and even death may occur following IPF and result in a significant financial burden [3]. Comorbidities including cardiac disease and gastroesophageal reflux [4] could further raise the risk of dying sooner.

According to epidemiological research, the fatality rate from fibrotic pulmonary dysfunction has reached 60%–70 % [5] since COVID-19. Glucocorticoids and cytotoxic medications are currently the mainstays of conventional IPF therapy, albeit their efficacy appears to be limited when used as an anti-IPF measure. Tyrosine kinase inhibitors, such as pirfenidone and nintedanib, which have received FDA approval, are being utilized as first-line treatments for IPF [6]. According to the data survey, the average expenses of nintedanib and pirfenidone for clinical treatment in the United States from 2014 to 2019 was USD 397.51 and USD 394.49, respectively. This indicates a low clinical utilization ratio, which is primarily attributable to the higher monthly amounts of self-paid patients. However, pirfenidone and nintedanib's potential medication side effects—gastrointestinal distress, skin eruption [7], diarrhea, and elevated liver enzymes [8]—avoid their widespread usage. Currently, lung transplantation [9] is the unique treatment that is known to improve the prognosis and increase survival for IPF patients, however, strategies that involve a limited number of appropriate IPF patients and a scarcity of donor organs have intrinsic advantages and disadvantages.

Recent studies have demonstrated that the intricate pathophysiology of IPF exhibits intertwined connection of cell types and signaling pathways, whereby the exploration of certain crucial signaling pathways serves as a catalyst for elucidating the IPF pathogenesis [10]. More medications, particularly Chinese medicinal formulae that target the anti-IPF signal pathways, have been verified in recent years. Herbal formulations have been demonstrated via numerous clinical studies to operate on the body through multi-component and multiple-target/pathway in order to combat respiratory disorders and improve the prognosis. To a greater extent, Traditional Chinese Medicine (TCM) is unable to realize modernization and globalization due to the mechanism of action and security are not sufficiently validated. A relatively new field, network pharmacology is intertwined with systems biology, genomics, polypharmacology, computational biology, and cutting-edge technologies integrated with massive data analysis and artificial intelligence. It has articulated the mechanism of disease and medicine function from the biological network [11], built a bridge between empirical and evidence-based medicine by constructing the “herb-compound-target-disease” relationship that was proposed by Professor Shao [12], and is thus appropriate for investigating pharmacological mechanisms in herbal formulas. Massive data sources would, however, induce a great deal of variation in the data algorithm. Other causes including acquisition from various databases and inconsistent standardization in data application [13] would generally result in deviations between predicted and the realistic constituents in holistic analysis as well.

Currently, there is no newly approved Chinese medicine for IPF treatment, leaving a significant gap in the field of treatment of this disease in China. With its origins in 40 years of clinical experience, Jinbei Oral Liquid (JBOL) is one of the few Chinese herbal medicine compounds specifically designed for the therapy of IPF. Multi-center clinical study findings have demonstrated that JBOL undoubtedly provides an advantage when it comes to considerably improving blood gas analysis, pulmonary function index, and blood oxygen saturation. In recent years, JBOL with unquestionable clinical efficacy and safety is frequently utilized at healthcare facilities as an approach to treating IPF [14]. JBOL consists of twelve herbs including *Angelica sinensis* (Oliv.) Diels, *Astragalus membranaceus* (Fisch.) Bge, *Codonopsis pilosula* (Franch.) Nannf, *Glycyrrhiza uralensis* Fisch, *Lonicera japonica* Thunb, *Glehnia littoralis* Fr. Schmidt ex Miq, *Pinellia ternata* (Thunb.) Breit, *Salvia miltiorrhiza* Bge, *Ligusticum striatum* DC, *Scutellaria baicalensis* Georgi, *Forsythia suspensa* (Thunb.) Vahl, and *Fritillaria cirrhosa* D. Don [15]. In order to precisely position the key components and targets, we have created a target network by utilizing realistic constituents rather than those that were predicted. We then imported the realistic constituents into the SwissTargetPrediction database and traditional Chinese medicine systems pharmacology (TCMSP) to investigate the hub genes in the biological information of JBOL that target IPF.

The goal of this study was to promote data mining of multi-component and multi-target via network pharmacology by analyzing realistic constituents as a benchmark. In order to confirm the inference of network pharmacology, we further investigated the crosstalk between ligand and protein of core components and targets using molecular docking and molecular dynamics simulation. In a nutshell, this research aims to offer a reference for methodically delving into the JBOL mechanism in anti-IPF using realistic ingredients.

2. Materials and methods

2.1. Screening the active ingredients and targets of JBOL

A total of 118 peaks were detected and identified [16] using ultra-high-performance liquid chromatography in conjunction with

quadruple time-of-flight mass spectrometry (UPLC-Q-TOF-MS). This mixture contained 43 flavonoids, 26 phenylpropanoids, 14 glycosides, 9 phthalides, 8 alkaloids, and other substances. The substances listed above that were assessed served as the research object. The databases SwissTargetPrediction (<http://www.swisstargetprediction.ch/>) and SwissADME (<http://www.swissadme.ch/>) [16] were utilized to uncover potential active ingredients and targets in JBOL, while the TCMSP database (<http://tcmspw.com/index.php>) [17,18] and literature mining were utilized to fill in the component targets that were left out of SwissTargetPrediction. The screening criteria for this study mainly include two indicators: OB \geq 30 % and DL \geq 0.1; GI absorption is “High” and DL index greater than or equal to 3 Yes; Probability \geq 0.1. Subsequently, the final targets set was uniformly encoded using UniProt (<https://www.uniprot.org/>) genes [19], which eliminated duplicates, using the species setting “*Homo sapiens*”, and the structures of the active compounds were summarized in Table 1.

2.2. Collection of the active ingredients-disease intersection targets

The target genes of IPF-related were retrieved with the keyword “Idiopathic pulmonary fibrosis”, “pulmonary fibrosis” in OMIM (<https://omim.org/>) [20], DisGeNET (<https://www.disgenet.org/>) and GeneCards (<https://www.genecards.org/>) databases [21,22]. The overlap between the targets of the active ingredient and the IPF-related targets was obtained using a Venn diagram, which was utilized to determine the potential therapeutic targets of IPF-related.

2.3. Construction of herb-active ingredient-target network

The active components of JBOL were matched to pertinent targets using the network biology visualization tool Cytoscape (3.10.1). To establish the herb-active ingredient-target network, the XLS files containing the node attribute information and node interaction connection were loaded into Cytoscape. The node size and (or) depth of color directly reflected the degree value of every node.

2.4. Construction of a PPI network diagram

Targets of ingredient-IPF intersection were loaded into the STRING database [23] (<https://string-db.org/>) to gather data on the protein interaction network. “*Homo sapiens*” was the criterion for screening the “organisms” and “medium confidence (0.4)” was the minimal required interaction score. The generated data was then extracted and loaded into Cytoscape (3.10.0) for the purpose to establish a PPI network. In the PPI network, the degree centrality (DC), closeness centrality (CC) [24], and betweenness centrality (BC) of the node are calculated, while the node size was visually represented according to DC. The key targets were extracted based on the degree value in the PPI network [25].

2.5. Genomic functional enrichment

Gene Ontology (GO) [26] and the Kyoto Encyclopedia of Genes and Genomes (KEGG) pathway enrichment analysis [27] were conducted out to obtain insight into the biological function of possible targets in IPF therapy using Metascape (<https://www.metascape.org>) database [28]. Molecular functions (MF), cellular components (CC), and biological processes (BP) were screened using GO analysis. Important signaling pathways involved in biological activities were identified by means of KEGG [29] enrichment analysis. During the analytic procedure, $p < 0.01$, minimum overlap of 3, and enrichment factor > 1.5 were collected and subsequently categorized based on how similar their members were. (last update date: 2024-02-19). For visual analysis, GO and KEGG data were uploaded to the Bioinformatics (<http://www.bioinformatics.com.cn/>).

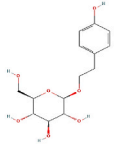
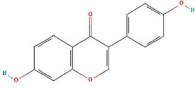
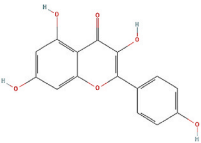
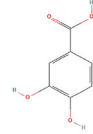
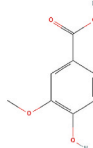
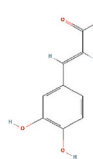
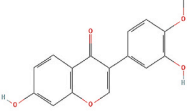
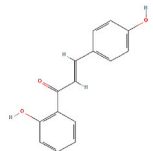
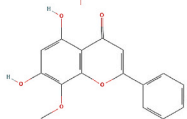
2.6. Construction of a ingredients-disease-target-pathway network

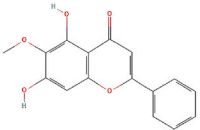
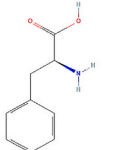
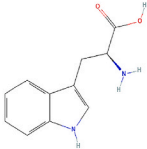
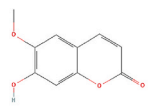
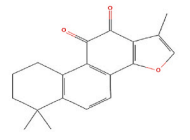
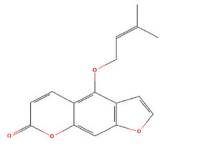
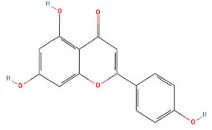
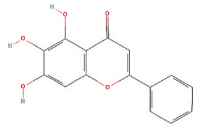
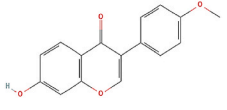
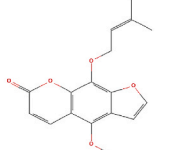
To further investigate the functional mechanism of JBOL’s active ingredients against IPF, the “ingredient-disease-target-pathway” network was constructed using the Cytoscape (3.10.1) software package [30] (Boston, MA, USA) to visualize and illuminate the intricate relationships between ingredients, targets, and pathways. The degree of every node in the network would be directly indicated by node size and/or color depth.

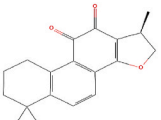
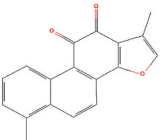
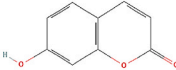
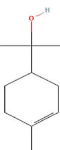
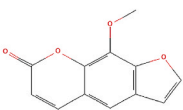
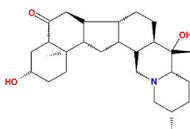
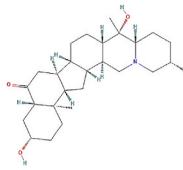
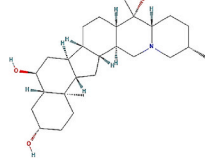
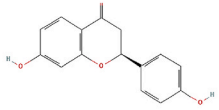
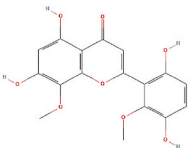
2.7. Molecular docking

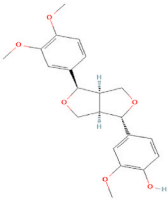
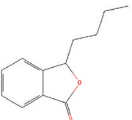
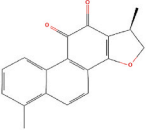
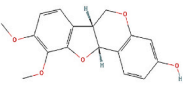
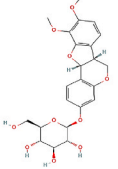
To verify the binding ability among the active ingredients and core target proteins, nine core ingredients were selected for molecular docking with nine target proteins [31]. We used AutoDock Vina for molecular docking, which adopted a semi-flexible docking mode [32]. The crystal structure of the core target proteins was made reference to RSCB PDB (<http://www.rcsb.org/>) [33]. The options of 3D structure need to coincide as follows: (1) the species type is “*Homo sapiens*”, (2) the pH of crystallization should approach the normal range of the human body, (3) Crystal proteins need to contain the information of original small molecule ligand, (4) High resolution ($\leq 2.5\text{\AA}$). The ligands and water molecules of each protein were removed by PyMOL software. The structure of the 3D files containing the active components was acquired using the PubChem database. The receptors and ligands were pretreated with hydrogenation using Auto Dock Tools 1.5.7 before docking, and the Grid Box was set with the original ligand as the center. The scope of the grid box should cover the entire protein receptor structure and ensure that any possible docking pockets are included. In order to assess free binding energies, AutoDock Vina was used for the docking process. Finally, we used the Discovery Studio (2024) and

Table 1
Prediction of the component of JBOL based on SwissADME and TCMSP.

NO.	Compound name	Molecular Formula	Molecular weight (g/mol)	2D structure	Degree	Betweenness Centrality	Closeness Centrality	Average Shortest Path Length	Herb
MOL002929	salidroside	C ₁₄ H ₂₀ O ₇	300.3		3	0.00003814	0.24562976	4.07116788	<i>Scutellaria baicalensis</i> Georgi
MOL000390	Daidzein	C ₁₅ H ₁₀ O ₄	254.24		55	0.03482508	0.36267373	2.75729927	<i>Astragalus membranaceus</i> (Fisch.) Bge
MOL000422	Kaempferol	C ₁₅ H ₁₀ O ₆	286.24		108	0.08847539	0.39059159	2.56021898	<i>Astragalus membranaceus</i> (Fisch.) Bge; <i>Salvia miltiorrhiza</i> Bge; <i>Lonicera japonica</i> Thunb.; <i>Forsythia suspensa</i> (Thunb.) Vahl.; <i>Glycyrrhiza uralensis</i> Fisch.
MOL000105	Protocatechuic acid	C ₇ H ₆ O ₄	154.12		16	0.00141689	0.31332190	3.19160584	<i>Salvia miltiorrhiza</i> Bge; <i>Lonicera japonica</i> Thunb.; <i>Pinellia ternata</i> (Thunb.) Breit; <i>Glycyrrhiza uralensis</i> Fisch
MOL000114	Vanillic acid	C ₈ H ₈ O ₄	168.15		40	0.05511525	0.31990660	3.12591241	<i>Astragalus membranaceus</i> (Fisch.) Bge; <i>Ligusticum striatum</i> DC; <i>Forsythia suspensa</i> (Thunb.) Vahl.; <i>Pinellia ternata</i> (Thunb.) Breit; <i>Glehnia littoralis</i> Fr. Schmidt ex Miq
MOL000414	Caffeic acid	C ₈ H ₆ O ₄	180.16		23	0.00503081	0.31953353	3.12956204	<i>Angelica sinensis</i> (Oliv.) Diels; <i>Lonicera japonica</i> Thunb.; <i>Forsythia suspensa</i> (Thunb.) Vahl.; <i>Astragalus membranaceus</i> (Fisch.) Bge; <i>Salvia miltiorrhiza</i> Bge
MOL000417	Calycosin	C ₁₆ H ₁₂ O ₅	284.26		24	0.00335723	0.33764633	2.96167883	<i>Glycyrrhiza uralensis</i> Fisch. <i>Astragalus membranaceus</i> (Fisch.) Bge
MOL001789	Isoliquiritigenin	C ₁₅ H ₁₂ O ₄	256.25		70	0.04470884	0.36902357	2.70985401	<i>Glycyrrhiza uralensis</i> Fisch
MOL000173	wogonin	C ₁₆ H ₁₂ O ₅	284.26		27	0.00692411	0.33723077	2.96532847	<i>Forsythia suspensa</i> (Thunb.) Vahl.; <i>Scutellaria baicalensis</i> Georgi

MOL002928	Oroxylin A	C ₁₆ H ₁₂ O ₅	284.26		53	0.01877551	0.36076366	2.77189781	<i>Scutellaria baicalensis</i> Georgi
MOL000041	phenylalanine	C ₉ H ₁₁ NO ₂	165.19		28	0.06109057	0.34837889	2.87043796	<i>Salvia miltiorrhiza</i> Bge
MOL001780	tryptophan	C ₁₁ H ₁₂ N ₂ O ₂	204.22		8	0.00511500	0.28736235	3.47992701	<i>Codonopsis pilosula</i> (Franch.) Nannf; <i>Glehnia littoralis</i> Fr. Schmidt ex Miq
MOL000040	scopoletin	C ₁₀ H ₈ O ₄	192.17		10	0.00072534	0.28796637	3.47262774	<i>Glehnia littoralis</i> Fr. Schmidt ex Miq; <i>Glycyrrhiza uralensis</i> Fisch <i>Angelica sinensis</i> (Oliv.) Diels; <i>Pinellia ternata</i> (Thunb.) Breit;
MOL007154	Tanshinone II A	C ₁₉ H ₁₈ O ₃	294.3		47	0.07874538	0.33764633	2.96167883	<i>Salvia miltiorrhiza</i> Bge
MOL001942	Isoimperatorin	C ₁₆ H ₁₄ O ₄	270.28		52	0.05636540	0.36123929	2.76824818	<i>Glehnia littoralis</i> Fr. Schmidt ex Miq; <i>Angelica sinensis</i> (Oliv.) Diels <i>Salvia miltiorrhiza</i> Bge;
MOL000008	Apigenin	C ₁₅ H ₁₀ O ₅	270.24		107	0.08581735	0.39114918	2.55656934	<i>Salvia miltiorrhiza</i> Bge; <i>Lonicera japonica</i> Thunb; <i>Scutellaria baicalensis</i> Georgi; <i>Codonopsis pilosula</i> (Franch.) Nannf
MOL002714	baicalein	C ₁₅ H ₁₀ O ₅	270.24		105	0.09308520	0.38782732	2.57846715	<i>Scutellaria baicalensis</i> Georgi; <i>Pinellia ternata</i> (Thunb.) Breit
MOL000392	formononetin	C ₁₆ H ₁₂ O ₄	268.26		58	0.03261330	0.36411960	2.74635036	<i>Glycyrrhiza uralensis</i> Fisch; <i>Astragalus membranaceus</i> (Fisch.) Bge
MOL002644	Phellopterin	C ₁₇ H ₁₆ O ₅	300.30		80	0.13457826	0.37457280	2.66970803	<i>Glehnia littoralis</i> Fr. Schmidt ex Miq

MOL007088	cryptotanshinone	C ₁₉ H ₂₀ O ₃	296.4		71	0.12474975	0.37052062	2.69890511	<i>Salvia miltiorrhiza</i> Bge
MOL007157	tanshinone i	C ₁₈ H ₁₂ O ₃	276.3		7	0.00417243	0.26333494	3.79744526	<i>Salvia miltiorrhiza</i> Bge
MOL003875	7-hydroxy coumarin	C ₉ H ₆ O ₃	162.14		68	0.09248614	0.36852724	2.71350365	<i>Angelica sinensis</i> (Oliv.) Diels
MOL010870	terpineol	C ₁₀ H ₁₈ O	154.25		3	0.00013533	0.27169063	3.68065693	<i>Lonicera japonica</i> Thunb; <i>Forsythia suspensa</i> (Thunb.) Vahl.
MOL001953	8-methoxypsoralen	C ₁₂ H ₈ O ₄	216.19		3	0.00010594	0.28088160	3.56021898	<i>Glehnia littoralis</i> Fr. Schmidt ex Miq
MOL009582	imperialine	C ₂₇ H ₄₃ NO ₃	429.6		67	0.06173069	0.35150738	2.84489051	<i>Fritillaria cirrhosa</i> D. Don
MOL004451	peiminine	C ₂₇ H ₄₃ NO ₃	429.6		68	0.06538033	0.35195890	2.84124088	<i>Fritillaria cirrhosa</i> D. Don
MOL004445	peimine(Verticine)	C ₂₇ H ₄₃ NO ₃	431.7		77	0.13540817	0.35105701	2.84854015	<i>Fritillaria cirrhosa</i> D. Don
MOL001792	liquiritigenin	C ₁₅ H ₁₂ O ₄	256.25		102	0.15498746	0.38618746	2.58941606	<i>Glycyrrhiza uralensis</i> Fisch
MOL002919	Viscidulin III	C ₁₇ H ₁₄ O ₈	346.3		8	0.00049205	0.31083381	3.21715328	<i>Scutellaria baicalensis</i> Georgi

MOL003330	Sylvatesmin	C ₂₁ H ₂₄ O ₆	372.4		28	0.03427274	0.33889920	2.95072993	<i>Forsythia suspensa</i> (Thunb.) Vahl.
61361	3-butylphthalide	C ₁₂ H ₁₄ O ₂	190.24		2	0.00364964	0.19564441	5.11131387	<i>Ligusticum striatum</i> DC
11425923	dihydrotanshinone I	C ₁₈ H ₁₄ O ₃	278.3		9	0.00142165	0.30461367	3.28284672	<i>Salvia miltiorrhiza</i> Bge
14077830	Methylissolin	C ₁₇ H ₁₆ O ₅	300.3		106	0.17915264	0.38727915	2.58211679	<i>Astragalus membranaceus</i> (Fisch.) Bge
101679160	Methylissolin-3-O-glucoside	C ₂₃ H ₂₆ O ₁₀	462.4		17	0.02290478	0.30908065	3.23540146	<i>Astragalus membranaceus</i> (Fisch.) Bge

PyMOL 2.5.8 (<https://www.pymol.org/>) to visualize and evaluate the interactions of typical docking data. The minimum binding energy among each pair of complexes was calculated to evaluate the binding stability between JBOL core components and target proteins. The binding energy value is inversely proportional to the binding ability, with binding energy ≤ -5 kcal/mol signifying strong binding activity [34].

2.8. Molecular dynamics simulation

Molecular dynamics simulations were run on the Amber 22 (San Francisco, CA, USA) to determine the binding mode and binding energy of the receptor protein with the lowest binding energy to the ligand during the molecular docking process. The ff19SB force field [35] was trained using TIP3P water, and counterions were added to neutralize the system. The system was heated up to 300 K within 500 ps when energy was minimized, and then the system achieved pre-equilibrated at 300 K using the regular system (NVT), lastly, molecular dynamics simulations were run for 100 ns at the isothermal isobaric system (NPT). The SHAKE limited all covalent bonds of hydrogen, and the results were analyzed with AmberTools23.

3. Results

3.1. Analysis of active components screening and target prediction

3.1.1. Prediction of nuclear ingredients combined with the realistic constituents

A total of 118 chemical ingredients of JBOL were identified through UPLC-Q-TOF-MS. In this investigation, 34 active compounds were screened according to the standards of SwissADME database systems, of which 14 components were shared by the 12 herbs. Including 8, 2, 6, 10, 4, 2, 5, 7, 6, 3, 4, and 6 compounds were obtained from HQ, DangS, BSS, DanS, DG, CX, JYH, LQ, HQIN, CBM, QBX, and GC, respectively. In addition, these substances contained two phenolic acids, five alkaloids, four tanshinones, seven phenylpropanols, and eleven flavonoids. The remaining compounds appertained to isoflavone, glycoside, phenylpropionic acid, and its derivatives, phthalide, and psoralen, respectively (Table 1). The UpSet plot acquired the information of intersecting components in 12 herbs and showed the amounts of active ingredients and common components distribution in each herb of JBOL (Fig. 1).

3.1.2. Construction of JBOL herb-active ingredient-target network

The herbs, active ingredients, and related putative targets of JBOL were entered into Cytoscape 3.10.1 to produce the herb-active ingredient-target network diagram (Fig. 2), which includes 549 nodes and 1550 edges. According to the network analysis tool, the network heterogeneity is 2.43 and the network centralization is 0.187. The top 10 active components with degree values were taken as the core nodes that including Kaempferol (MOL000422, degree:108), Apigenin (MOL000008, degree:107), Methylnissoin (14077830, degree:106), Baicalein (MOL002714, degree:105), Liquiritigenin (MOL001792, degree:102), Phellopterin (MOL002644, degree:80), Peimine (MOL004445, degree:77), Cryptotanshinone (MOL007088, degree:71), Isoliquiritigenin (MOL001789, degree:70), 7-hydroxy coumarin (MOL003875, degree:68). The network revealed that the most significant active ingredients interacting with the targets were kaempferol, apigenin, methylnissoin, and baicalein, among others.

3.2. Prediction of potential targets of JBOL in the treatment of IPF

The retrieval terms were set to “Idiopathic Pulmonary Fibrosis”, “Pulmonary Fibrosis”, and the condition was set to “*Homo sapiens*”. The targets associated to IPF were found using the DisGeNET, GeneCards, and OMIM databases. The findings indicated that 1708, 1671, and 356 were the confirmed or potential IPF targets, respectively. Uniprot was applied to the screen and standardized all disease targets with corresponding gene symbols. A total of 1169 targets were extracted after deduplication. According to the Venn diagram data, a total of 122 intersection targets between JBOL component targets and IPF disease. The Venn diagram data indicates that there are 122 intersection targets between IPF targets and JBOL component targets (Fig. 3).

3.3. PPI network construction and core target selection

We entered 122 common targets to the STRING database into create a PPI network with the aim to investigate the mechanism potential therapeutic effects of JBOL against IPF (Fig. 4A). Proteins were represented by nodes, while protein associations were displayed via lines. The network displayed 120 nodes and 1793 edges, with median DC values of 26. Based on topology analysis, the core PPI network was identified, with $DC \geq 2$ times the median and $DC, BC, \text{ and } CC \geq \text{median}$ as the screening criterion. Topological analysis indicated that 8 core objectives stand out distinctly. (Table 2 and Fig. 4A), namely RAC-alpha serine/threonine-protein kinase (AKT1), Epidermal growth factor receptor (EGFR), Proto-oncogene tyrosine-protein kinase Src (SRC), Signal transducer and activator of transcription 3 (STAT3), Matrix metalloproteinase-9 (MMP9), mitogen-activated protein kinase 3 (MAPK3), Caspase-3 (CASP3) and Heat shock protein HSP 90-alpha (HSP90AA1) (Table 2). The network with essential and non-essential targets was constructed

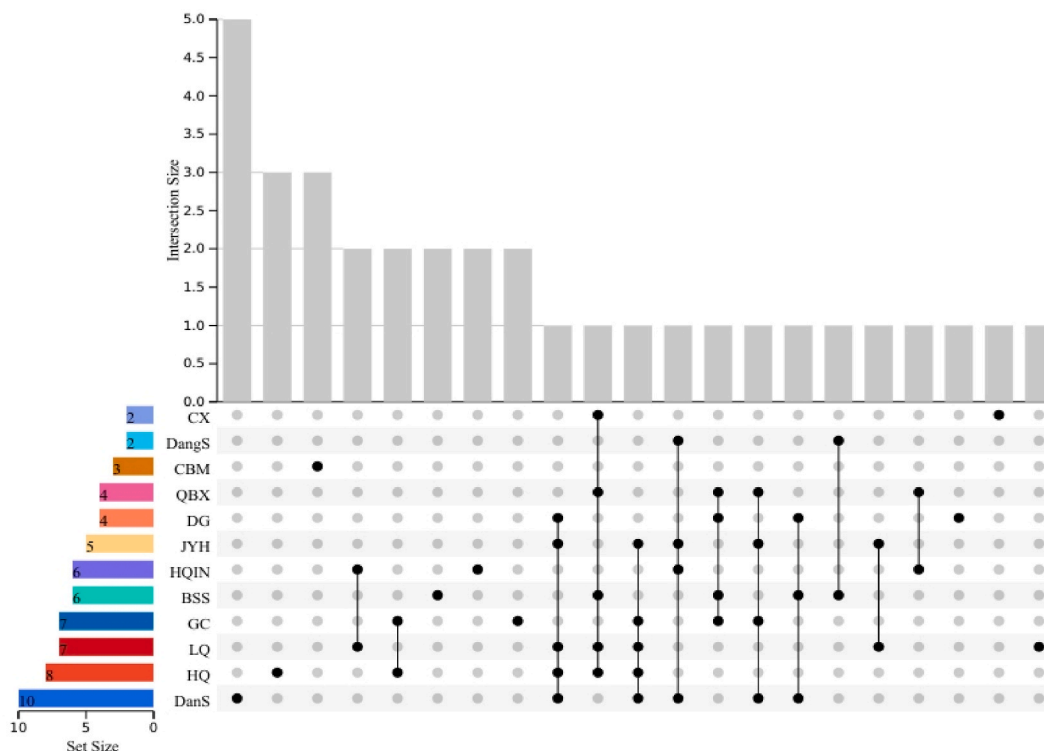


Fig. 1. Distribution of the predicted active ingredients in 12 herbs. The number of active compounds found in every herb is indicated in the strip at the bottom left. The intersection situations of the individual sets are displayed by the dots and lines at the bottom right. A histogram illustrates the quantity of relevant components exist in each subset.

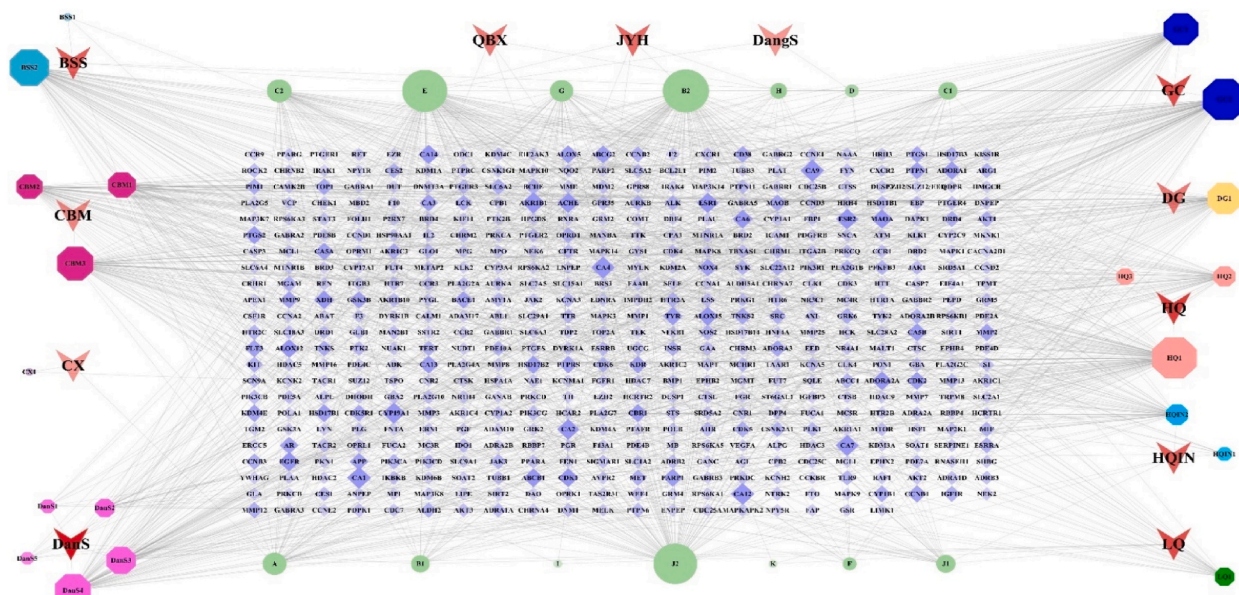


Fig. 2. Herb-active ingredient-target network of JBOL. (Red arrows represent the herbs in JBOL, the octagon node represents components of JBOL, 2 blue octagon nodes are BSS compounds, 3 crimson octagon nodes are CBM compounds, 1 purple octagon node is CX compound, 5 rose red octagon nodes are DanS compounds, 2 navy blue octagon nodes are GC compounds, 1 yellow octagon node is DG compound, 3 Red octagon nodes are HQ compounds, 2 blue octagon nodes are CX compounds, 1 bottle-green octagon node is LQ compound, and the 14 light green circular nodes are common components in the twelve herbs of JBOL. Purple rhombus node represent predict targets. The edges depict the interaction between ingredients and targets, and the node size and depth of color are proportional to the degree value of interaction.

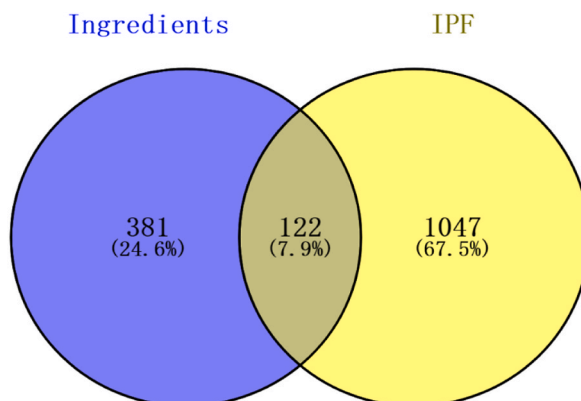


Fig. 3. Venn diagram of the target of JBOL and the target of IPF.

simultaneously (Fig. 4B), with node sizes in this network proportional to the target degree.

3.4. GO enrichment and KEGG pathway analysis

The core targets were imported into the Metascape database for enrichment analysis. The top 10 items of biological function (BP), cell function (CC), and molecular function (MF) ($P < 0.01$) in GO analysis were shown in Fig. 5. Among them, BP involved positive regulation of phosphorus and phosphate, transmembrane receptor protein tyrosine kinase signaling pathway, positive regulation of protein phosphorylation, transferase, and kinase activity. There were vesicle lumen, caveola, membrane raft, membrane microdomain, and focal adhesion. In CC, MF was related to protein kinase activity and phosphotransferase activity with the alcohol group as acceptor, kinase activity, protein tyrosine kinase activity, and transmembrane receptor protein tyrosine kinase activity.

The first 20 signal pathways involved pathways in cancer, AGE-RAGE signaling pathway, lipid and atherosclerosis, EGFR tyrosine kinase inhibitor resistance PI3K-Akt signaling pathway, and so on (Table 3 and Fig. 6A and B). Using the Bioinformatics platform (<http://www.bioinformatics.com.cn/>), a Sankey diagram was established on the basis of the relationship between the target genes and

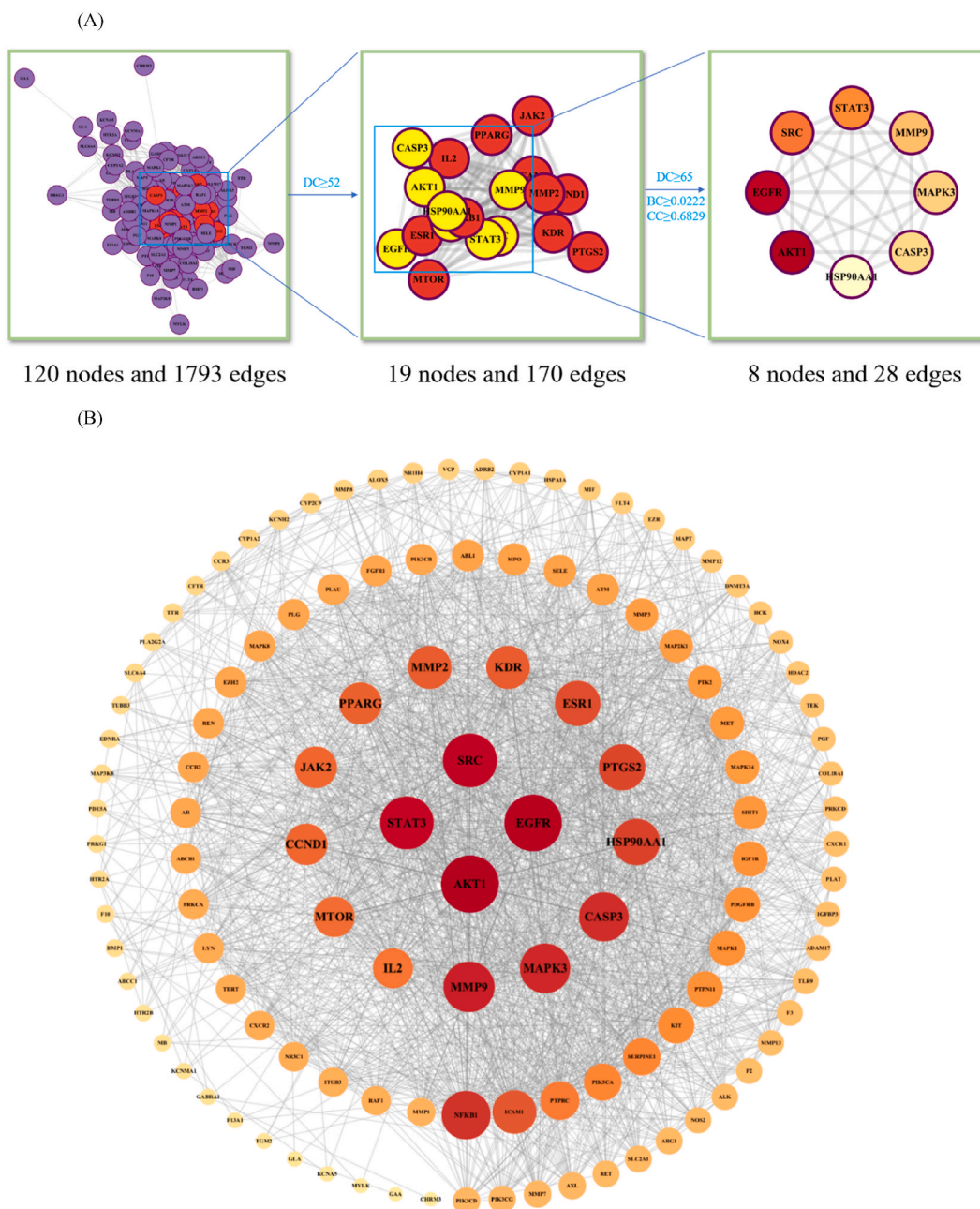


Fig. 4. The PPI network of JBOL and IPF predict key targets. (A) The PPI network screening process. The 8 core targets were screened by screening from 122 common targets via the value of DC, BC, and CC. (B) Construction of core target and non-core target network. Nodes represent proteins (The important target is indicated by the red circular node; the node size and color depth are graphically depicted based on the DC value.), edge represents protein-protein association.

the enrichment pathways (Fig. 6C).

3.5. Construction of JBOL ingredients-disease-target-pathway network

Finally, we constructed a ingredients-disease-target-pathway network and visualized using Cytoscape 3.10.1 (Fig. 7), containing 185 nodes and 905 edges. The degree value indicated that kaempferol, apigenin, baicalein, vanillic acid, and isoimperatorin were the top 5 active components. The top five targets included EGFR, AKT1, PIK3CA, PIK3CD and MAP2K1.

Table 2
Core targets information of PPI network.

UniProt ID	Gene symbol	Protein name	Degree	Betweenness Centrality	Closeness Centrality
P31749	AKT1	RAC-alpha serine/threonine-protein kinase	87	0.0628	0.7778
P00533	EGFR	Epidermal growth factor receptor	86	0.0599	0.7727
P12931	SRC	Proto-oncogene tyrosine-protein kinase Src	80	0.0761	0.7438
P40763	STAT3	Signal transducer and activator of transcription 3	79	0.0284	0.7391
P14780	MMP9	Matrix metalloproteinase-9	74	0.0309	0.7169
P27361	MAPK3	Mitogen-activated protein kinase 3	72	0.0261	0.7083
P42574	CASP3	Caspase-3	71	0.0222	0.7041
P07900	HSP90AA1	Heat shock protein HSP 90-alpha	66	0.0669	0.6879

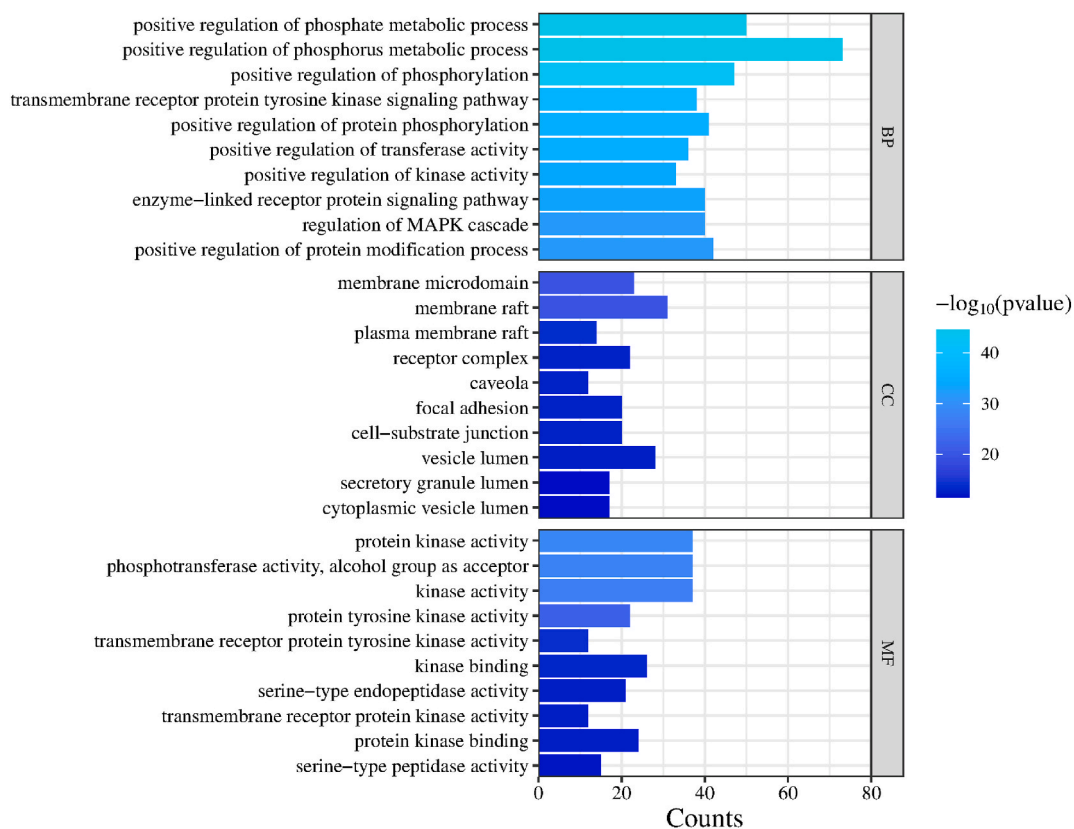


Fig. 5. GO analysis (Top 10 terms of biological process (BP), molecular function (MF) and cellular component (CC)).

3.6. Analysis of molecular docking

Molecular docking was used to evaluate the interaction of screening active ingredients and core targets to validate the findings from network pharmacology. Based on synthesis analysis of the degree values from the PPI network and KEGG, 9 key protein targets were chosen. 9 active components that achieved high degree values through the “herb-active ingredient-targets” network was used for molecular docking. Realistic ingredients with high contents from previous experiments were also taken into account. Based on the aforementioned outcome, we docked 9 receptor proteins-AKT1 (PDB ID: 4EJN), EGFR (PDB ID: 4LQM), SRC (PDB ID: 1T65), STAT3 (PDB ID: 5AX3), MMP9 (PDB ID: 4WZV), MAPK3 (PDB ID: 2ZOP), CASP3 (PDB ID: 3KJF), HSP90AA1 (PDB ID: 5VYY), MTOR (PDB ID: 4DRI)-with 9 ingredients as ligands, including kaempferol, apigenin, methylchlopiquinone, baicalein, liquiritigenin, phellopterin, peimine, cryptotanshinone, and wogonin. An average free binding energy value of -8.27 kcal-mol⁻¹ was found in the docking results of 81 groups of active ingredient-target protein, indicating tight binding activity in screening active components with core targets (Fig. 8). The top eight compound-target interactions and the binding mode with the highest free binding energy score were visualized using PyMol2.5.8 and Discovery Studio 2024 (Fig. 9 and Table 4).

The smaller the value of the binding free energy, the lower the binding free energy and the stronger the binding. A ligand would demonstrate a certain binding activity, a satisfactory binding activity, and a tight binding activity with the receptor if its binding energy was less than -4.25 kcal-mol⁻¹, -5.0 kcal-mol⁻¹, and -7.0 kcal-mol⁻¹, respectively [36]. Out of all of them, the free binding

Table 3
Analysis of the KEGG pathway of phillygenin for weight loss (Top 20).

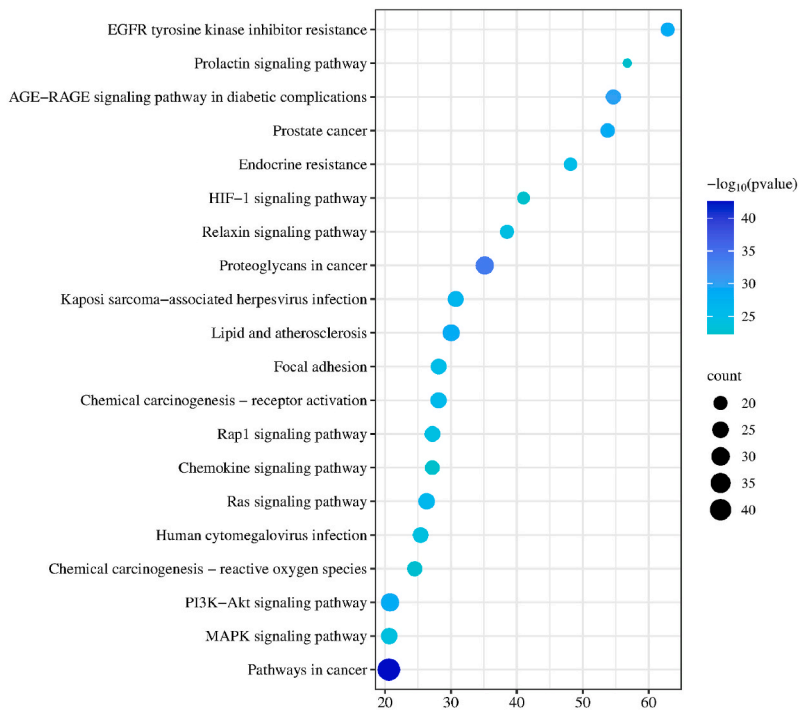
ID	Description	Count	Gene ID	P-Value
hsa05200	Pathways in cancer	44	ABL1, AKT1, ALK, AR, CCND1, CASP3, EDNRA, EGFR, ESR1, F2, FGFR1, FLT4, MTOR, HDAC2, HSP90AA1, IGF1R, IL2, JAK2, KIT, MET, MMP1, MMP2, MMP9, NFKB1, NOS2, PDGFRB, PGF, PIK3CA, PIK3CB, PIK3CD, PPARG, PRKCA, MAPK1, MAPK3, MAPK8, MAP2K1, PTGS2, PTK2, RAF1, RET, SLC2A1, STAT3, TERT, VEGFA	2.96E-43
hsa04151	PI3K-Akt signaling pathway	30	AKT1, CCND1, EGFR, FGFR1, FLT4, MTOR, HSP90AA1, IGF1R, IL2, ITGB3, JAK2, KDR, KIT, MET, NFKB1, PDGFRB, PGF, PIK3CA, PIK3CB, PIK3CD, PIK3CG, PRKCA, MAPK1, MAPK3, MAP2K1, PTK2, RAF1, RET, TEK, VEGFA	2.73E-29
hsa05205	Proteoglycans in cancer	29	AKT1, CCND1, CASP3, MAPK14, EGFR, ESR1, FGFR1, MTOR, IGF1R, ITGB3, KDR, MET, MMP2, MMP9, PIK3CA, PIK3CB, PIK3CD, PLAU, PRKCA, MAPK1, MAPK3, MAP2K1, PTK2, PTPN11, RAF1, SRC, STAT3, VEGFA, EZR	1.55E-34
hsa05417	Lipid and atherosclerosis	26	AKT1, CASP3, MAPK14, CYP11A1, CYP2C9, HSPA1A, HSP90AA1, ICAM1, JAK2, LYN, MMP1, MMP3, MMP9, NFKB1, PIK3CA, PIK3CB, PIK3CD, PPARG, PRKCA, MAPK1, MAPK3, MAPK8, PTK2, SELE, SRC, STAT3	2.73E-29
hsa04014	Ras signaling pathway	25	ABL1, AKT1, EGFR, FGFR1, FLT4, IGF1R, KDR, KIT, MET, NFKB1, PDGFRB, PGF, PIK3CA, PIK3CB, PIK3CD, PLA2G2A, PRKCA, MAPK1, MAPK3, MAPK8, MAP2K1, PTPN11, RAF1, TEK, VEGFA	6.44E-27
hsa04010	MAPK signaling pathway	25	AKT1, CASP3, MAP3K8, MAPK14, EGFR, FGFR1, FLT4, HSPA1A, IGF1R, KDR, KIT, MAPT, MET, NFKB1, PDGFRB, PGF, PRKCA, MAPK1, MAPK3, MAPK8, MAP2K1, RAF1, RET, TEK, VEGFA	1.82E-24
hsa05167	Kaposi sarcoma-associated herpesvirus infection	24	AKT1, CCND1, CASP3, CCR3, MAPK14, MTOR, HCK, ICAM1, JAK2, LYN, NFKB1, PIK3CA, PIK3CB, PIK3CD, PIK3CG, MAPK1, MAPK3, MAPK8, MAP2K1, PTGS2, RAF1, SRC, STAT3, VEGFA	2.03E-27
hsa05207	Chemical carcinogenesis-receptor activation	24	ADRB2, AKT1, AR, CCND1, CHRNA7, CYP1A1, CYP1A2, EGFR, ESR1, MTOR, HSP90AA1, JAK2, NFKB1, PIK3CA, PIK3CB, PIK3CD, PRKCA, MAPK1, MAPK3, MAP2K1, RAF1, SRC, STAT3, VEGFA	1.51E-26
hsa04510	Focal adhesion	23	AKT1, CCND1, EGFR, FLT4, IGF1R, ITGB3, KDR, MET, MYLK, PDGFRB, PGF, PIK3CA, PIK3CB, PIK3CD, PRKCA, MAPK1, MAPK3, MAPK8, MAP2K1, PTK2, RAF1, SRC, VEGFA	1.76E-25
hsa04015	Rap1 signaling pathway	23	AKT1, MAPK14, EGFR, FGFR1, FLT4, IGF1R, ITGB3, KDR, KIT, MET, PDGFRB, PGF, PIK3CA, PIK3CB, PIK3CD, PRKCA, MAPK1, MAPK3, MAP2K1, RAF1, SRC, TEK, VEGFA	3.64E-25
hsa05163	Human cytomegalovirus infection	23	AKT1, CCND1, CASP3, CCR3, MAPK14, EGFR, MTOR, CXCR2, ITGB3, NFKB1, PIK3CA, PIK3CB, PIK3CD, PRKCA, MAPK1, MAPK3, MAP2K1, PTGS2, PTK2, RAF1, SRC, STAT3, VEGFA	1.62E-24
hsa04933	AGE-RAGE signaling pathway in diabetic complications	22	AKT1, CCND1, CASP3, MAPK14, F3, ICAM1, JAK2, MMP2, NFKB1, SERPINE1, PIK3CA, PIK3CB, PIK3CD, PRKCA, PRKCD, MAPK1, MAPK3, MAPK8, SELE, STAT3, VEGFA, NOX4	1.39E-30
hsa05208	Chemical carcinogenesis-reactive oxygen species	22	ABL1, AKT1, MAPK14, CYP1A1, CYP1A2, EGFR, MET, NFKB1, PIK3CA, PIK3CB, PIK3CD, PRKCD, MAPK1, MAPK3, MAPK8, MAP2K1, PTK2, PTPN11, RAF1, SRC, VEGFA, NOX4	4.01E-23
hsa05215	Prostate cancer	21	AKT1, AR, CCND1, EGFR, FGFR1, MTOR, HSP90AA1, IGF1R, MMP3, MMP9, NFKB1, PDGFRB, PIK3CA, PIK3CB, PIK3CD, PLAT, PLAU, MAPK1, MAPK3, MAP2K1, RAF1	2.86E-29
hsa04062	Chemokine signaling pathway	21	AKT1, CCR3, HCK, CXCR1, CXCR2, JAK2, LYN, NFKB1, PIK3CA, PIK3CB, PIK3CD, PIK3CG, PRKCD, MAPK1, MAPK3, MAP2K1, PTK2, RAF1, SRC, STAT3, CCR2	4.73E-23
hsa01521	EGFR tyrosine kinase inhibitor resistance	20	AKT1, AXL, EGFR, MTOR, IGF1R, JAK2, KDR, MET, PDGFRB, PIK3CA, PIK3CB, PIK3CD, PRKCA, MAPK1, MAPK3, MAP2K1, RAF1, SRC, STAT3, VEGFA	2.73E-29
hsa04926	Relaxin signaling pathway	20	AKT1, MAPK14, EGFR, MMP1, MMP2, MMP9, MMP13, NFKB1, NOS2, PIK3CA, PIK3CB, PIK3CD, PRKCA, MAPK1, MAPK3, MAPK8, MAP2K1, RAF1, SRC, VEGFA	5.76E-25
hsa01522	Endocrine resistance	19	AKT1, CCND1, MAPK14, EGFR, ESR1, MTOR, IGF1R, MMP2, MMP9, PIK3CA, PIK3CB, PIK3CD, MAPK1, MAPK3, MAPK8, MAP2K1, PTK2, RAF1, SRC	1.42E-25
hsa04066	HIF-1 signaling pathway	18	AKT1, EGFR, MTOR, IGF1R, NFKB1, NOS2, SERPINE1, PIK3CA, PIK3CB, PIK3CD, PRKCA, MAPK1, MAPK3, MAP2K1, SLC2A1, STAT3, TEK, VEGFA	4.73E-23
hsa04917	Prolactin signaling pathway	16	AKT1, CCND1, MAPK14, ESR1, JAK2, NFKB1, PIK3CA, PIK3CB, PIK3CD, MAPK1, MAPK3, MAPK8, MAP2K1, RAF1, SRC, STAT3	5.56E-23

energy of MTOR with peimine exhibited the highest affinity, it was $-11.1 \text{ kcal mol}^{-1}$. The interaction was mainly reflected in the formation of hydrogen bonds with TYR-57, and ARG-73 residues and hydrophobic interactions with TRP-2102, TRY-2105, PHE-77, ILE-87, VAL-86, PHE-2039, and PHE-2108 residues of MTOR. Other groups of target protein-active ingredient, like apigenin-MMP9 and cryptotanshinone-AKT1, also exhibited high free binding energies, all of which were less than $-9.4 \text{ kcal mol}^{-1}$. Additionally, this investigation discovered that MMP9 could interact with apigenin, kaempferol, baicalein, liquiritigenin, and wogonin, among additional compounds. The interaction was concerned with the formation of hydrogen bonds and hydrophobic interactions, whose residues included ALA-189, VAL-223, etc. We predicted that screening compounds and targets would be important in the management of IPF based on the aforementioned findings. It should be mentioned, nonetheless, that more experimental verification is required for the potential active components.

3.7. Molecular dynamic simulation

The molecular dynamic simulation was run to investigate the binding abilities of AKT1 to cryptotanshinone, MTOR to peimine, and MMP9 to apigenin. Root Mean Square Fluctuation (RMSD) curves of protein indicated position variability between the conformation

(A)



(B)

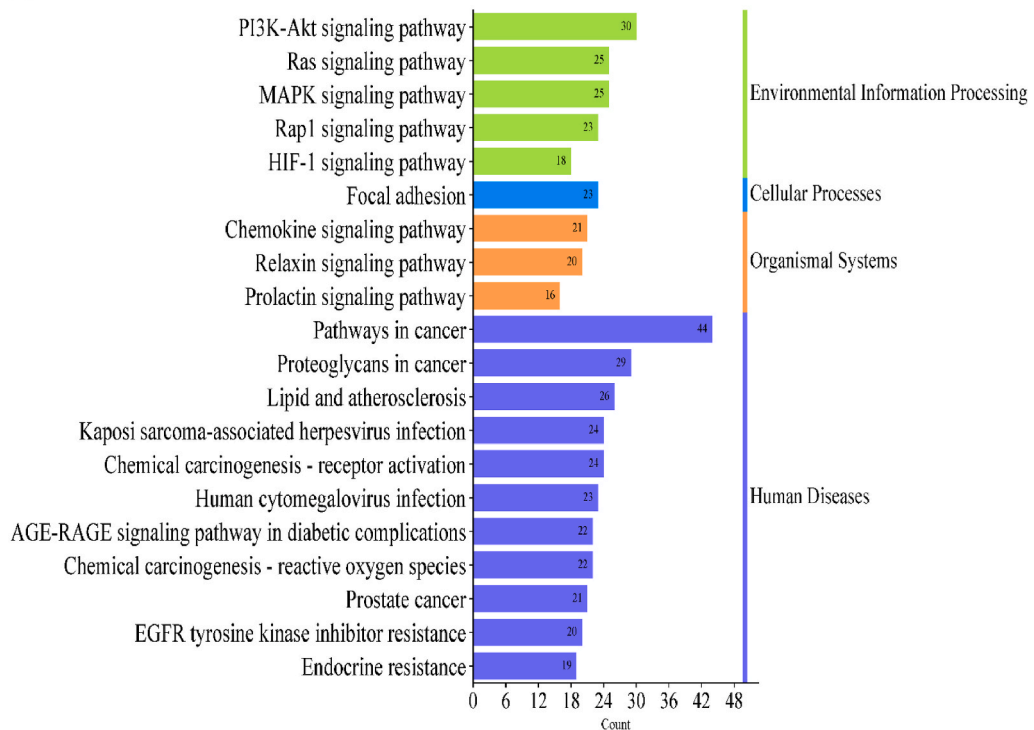


Fig. 6. Results of KEGG pathway enrichment analysis. (A) The bubble diagram for the top 20 pathways in the KEGG enrichment analysis. (B) The KEGG type of the top 20 pathways. (C) The KEGG enrichment analysis sankey diagram for the JBOL anticipated targets in the anti-IPF. The KEGG pathways are symbolized via the right rectangle nodes in the sankey diagram, the anticipated targets via the left rectangle nodes, and the interaction

between the target and the pathway with the lines. The right side is a conventional bubble diagram. The bubble size represents the number of genes to which the pathway belongs, and the bubble color represents the p -value.

(C)

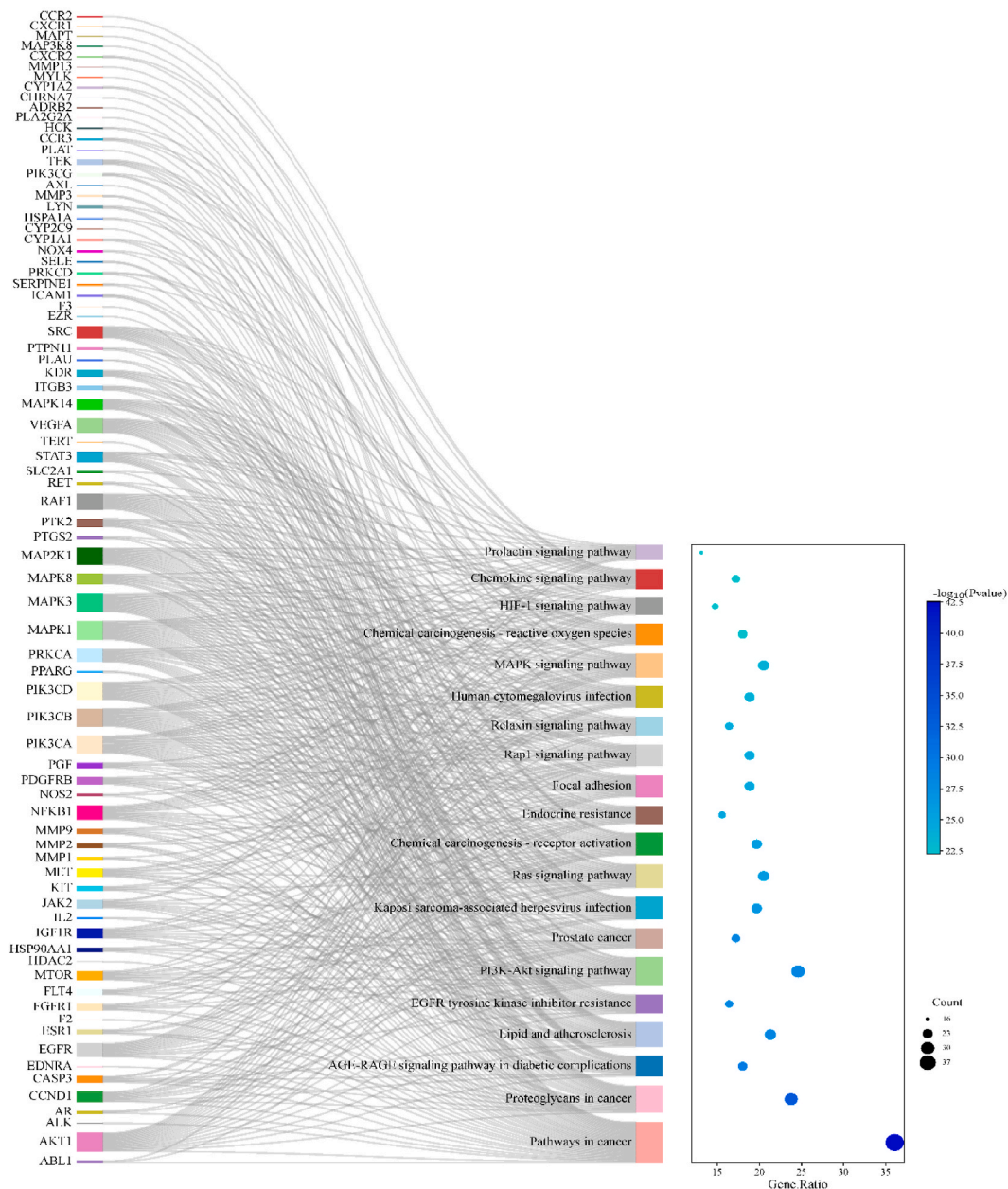


Fig. 6. (continued).

and initial conformation during the MD simulation. As shown in Fig. 10. The protein structures of peimine-MTOR and apigenin-MMP9 were stable after 40 ns, cryptotanshinone- AKT1 remained more stable after 60 ns, which signified the protein structure of three complexes showed a slight modification, but the bindings were mostly stable. The fact that the RMSD curve was not disrupted indicated that the core chemicals might remain tightly linked to screened proteins throughout the simulation without separating from the protein pocket.

The quantity of hydrogen bonding in the protein-compound interactions assessed the binding strength, the strongest and most dense hydrogen bonds were found in peimine-MTOR among them. According to MM/PBSA calculations, binding free energy represents the stability and variation of ligand and binding protein properties. The total binding free energies of peimine-MTOR,

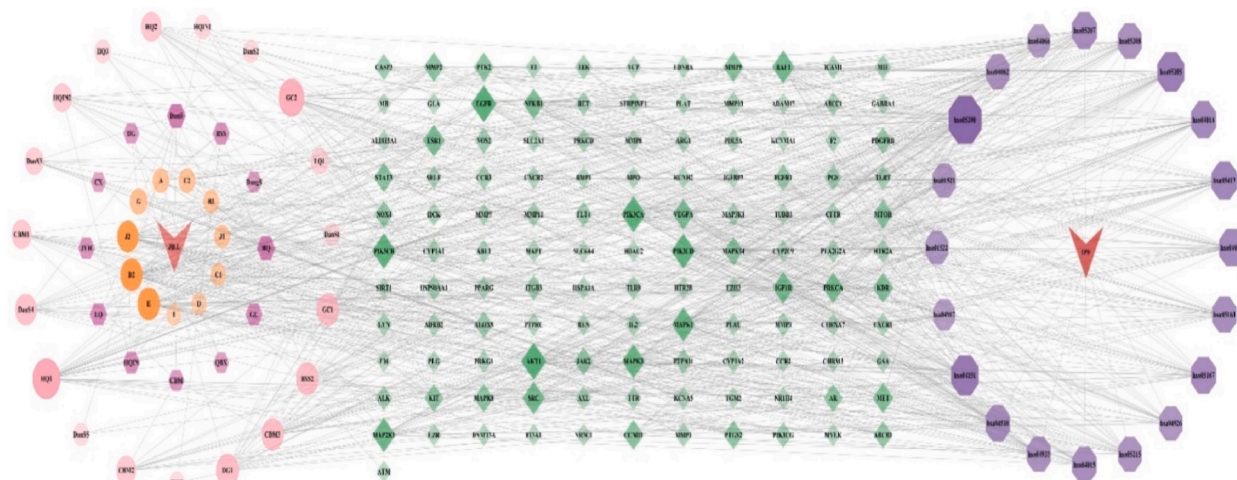


Fig. 7. The ingredients-disease-target-pathway network of JBOL in ant-IPF. The green rhombus nodes represent the targets, the lavender hexagon nodes represent the herb, the pink circle nodes represent the ingredients, orange circle nodes represent the common ingredients, the purple octagon nodes represent the pathways.

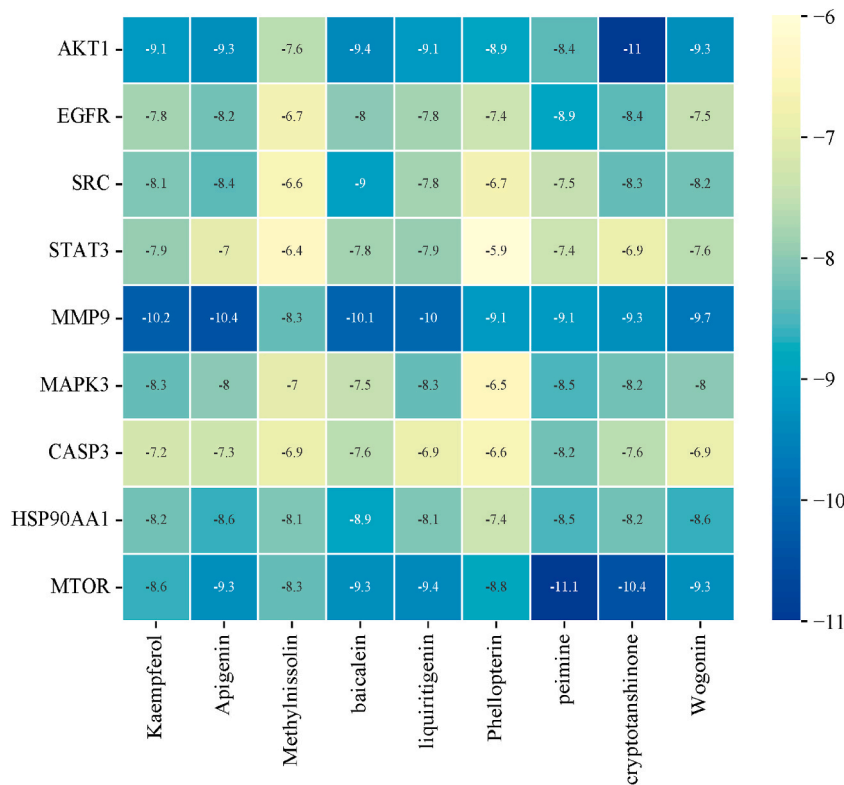
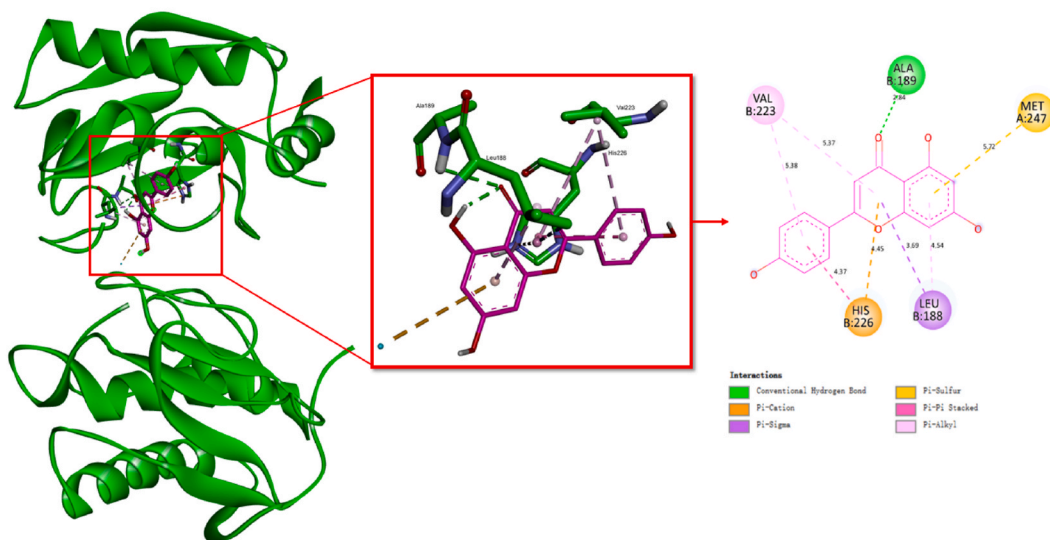


Fig. 8. Heat map of Molecular docking binding energy.

cryptotanshinone-AKT1, and apigenin-MMP9 were -37.78 , -33.36 , and -21.44 kJ/mol, respectively. Peimine-MTOR exhibited the lowest binding free energy and the maximum binding intensity, in agreement with the outcomes of molecular docking and dynamic simulation.

(A)



(B)

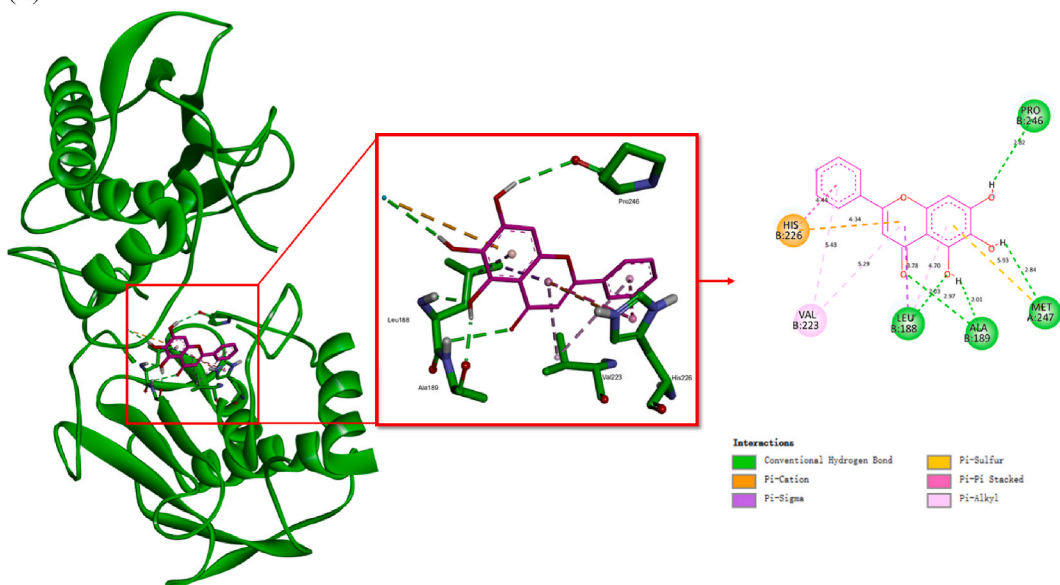


Fig. 9. Molecular docking mode of core targets and screened active ingredients: Apigenin-MMP9 (A), baicalein-MMP9 (B), cryptotanshinone-AKT1 (C), cryptotanshinone-MTOR (D), kaempferol-MMP9 (E), liquiritigenin-MMP9 (F), peimine-MTOR (G), wogonin-MMP9 (H).

4. Discussion

The development of pulmonary fibrosis is associated with the stimulation of inflammatory cytokines and the promotion of the epithelial-mesenchymal transition (EMT), which are both aided by the significant upregulation of alveolar epithelial cells and vascular endothelial cells in hyperplastic during the course of IPF [37]. Moreover, it involves the following: angiogenesis, oxidative stress, extracellular matrix deposition, insufficient autophagy, immune response misaligned, imbalance of the coagulation and fibrinolysis systems, etc. [38]. In some instances, the above-mentioned provides future directions of treatment, prevention in clinical practice of anti-fibrosis. Modern medicine has not by any means clarified the pathophysiology of IPF. Patients still have unmet medical demands despite the wide range of conventional medication alternatives available for the management of IPF because they don't feel satisfied

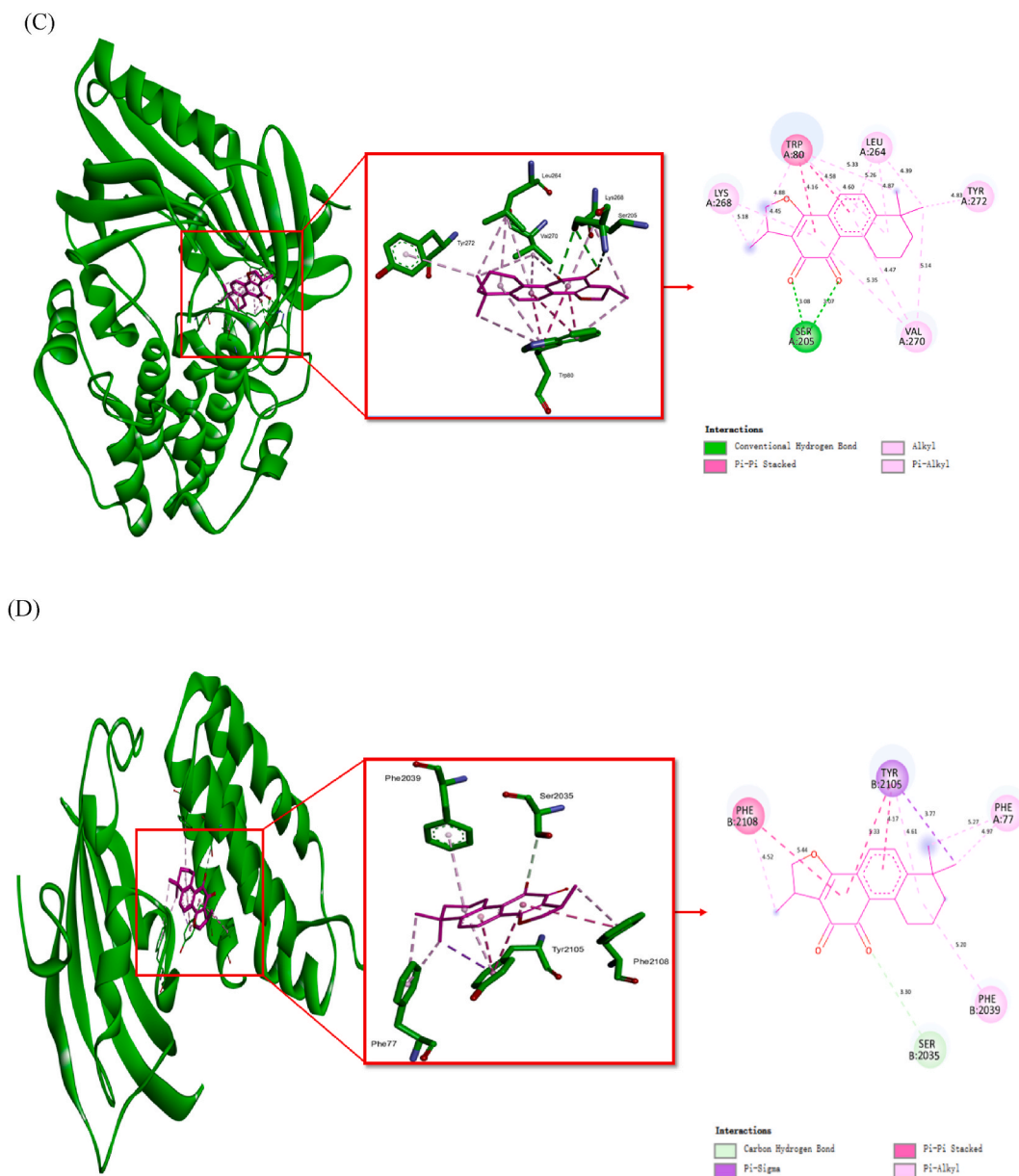
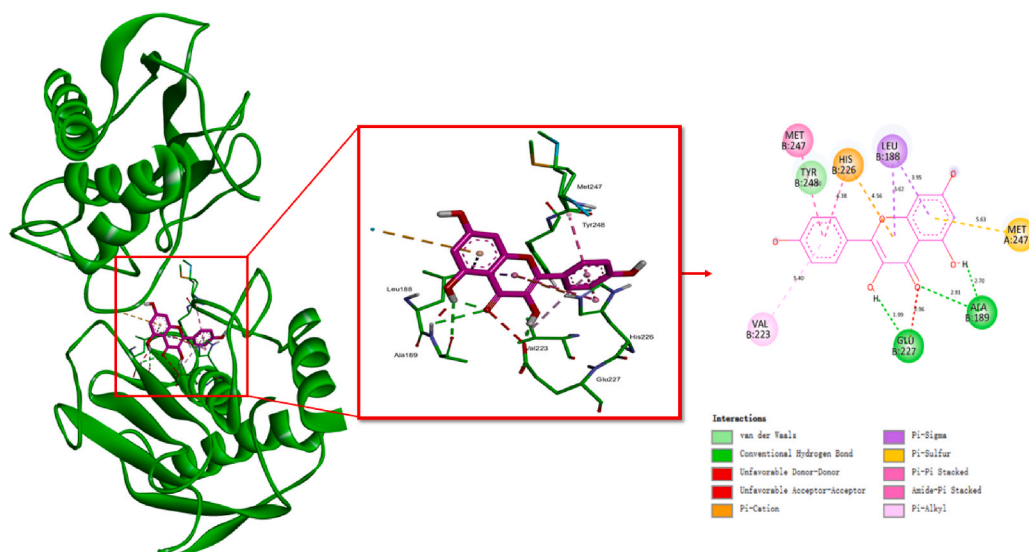


Fig. 9. (continued).

with their treatment or stick with it. The application of TCM, particularly with regard to the use of herbs or extracts from them, has garnered significant attention in the wake of its exceptional efficiency in treating COVID-19. TCM classifies the IPF into two categories: “pulmonary flaccidity” and “pulmonary arthralgia” [39]. The pathophysiology of “pulmonary flaccidity” and “pulmonary arthralgia” is described in ancient medical literature as being characterized by an embodied deficiency of vital qi, blood and qi stagnation, and phlegm stasis blocking [40]. The principles of TCM include replenishing qi and nourishing yin, activating blood and dredging collaterals, and resolving phlegm and masses as the entry point to resist IPF.

On the other hand, there are rarely any reports on the range of TCM preparations that have obvious advantages in treating IPF. JBOL is a hospital prescription that was developed based on clinical experience. It possessed the advantage in therapy of pulmonary interstitial fibrosis and acute lung injury, some of which benefits include replenishing qi and nourishing yin, clearing heat and detoxifying and relieving cough, and resolving phlegm. Prior multi-center clinical trials have demonstrated that JBOL provides unique clinical treatment advantages with a notable improvement in lung function indicators and blood gas analysis, suggesting that JBOL might be an additional therapeutic scheme option for the treatment of IPF. A prior study revealed that JBOL prevented the production of inflammatory factors, which in turn helped to ameliorate bleomycin-induced IPF in rats. Anti-IPF was also validated by JBOL inhibiting EMT *in vitro* experiment [41] and downregulating the expression of ERK1/2, JNK, and p38 by decreasing phosphorylation

(E)



(F)

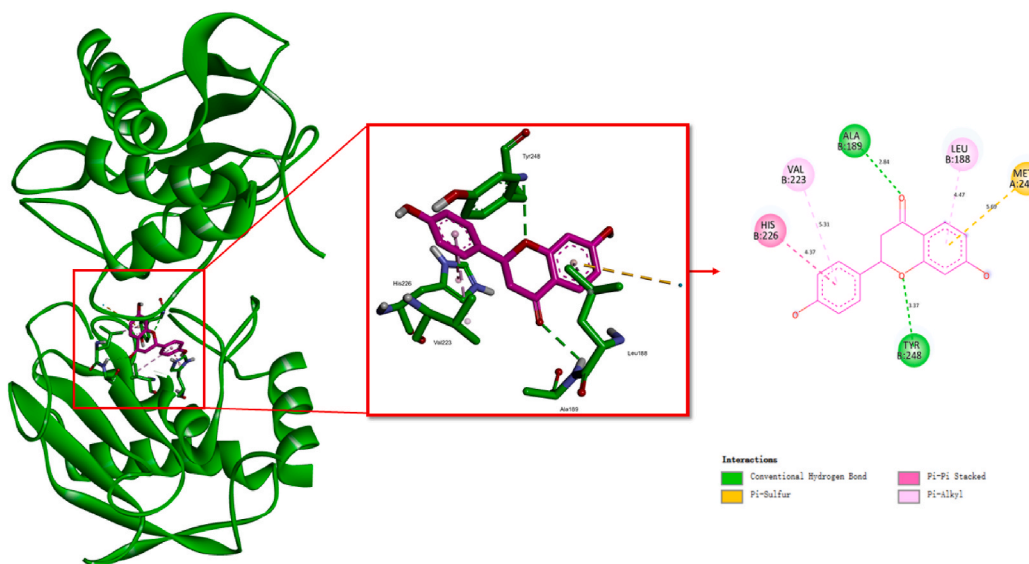
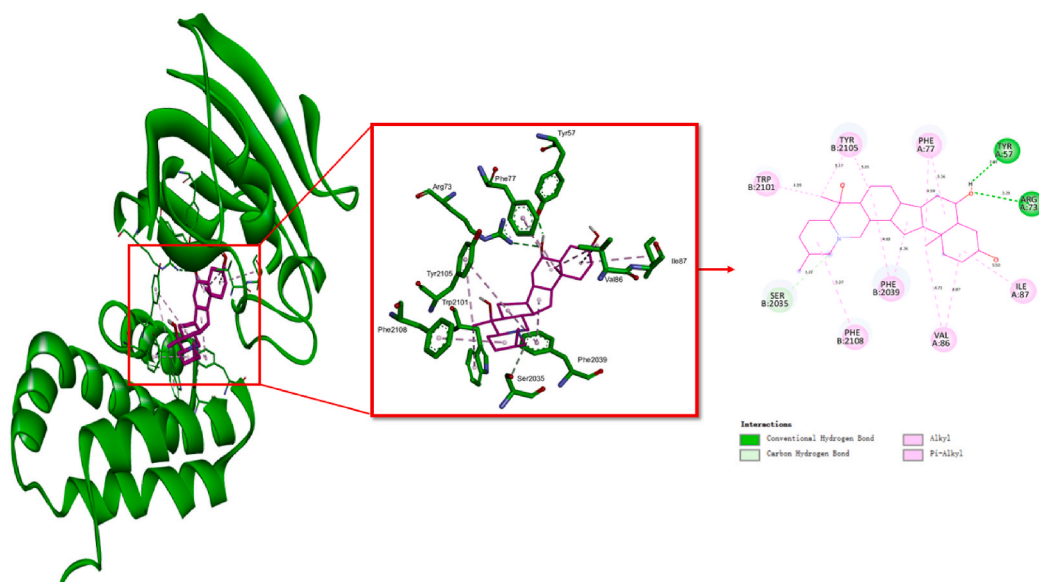


Fig. 9. (continued).

[42]. All these results indicate that JBOL plays a critical role in anti-IPF with multiple components and pathways. Nevertheless, data mining and experimental validation are still required for active components and mechanisms. It is critical for the determination of the key indicators to ensure their safety and efficacy in clinical use. In order to lay the groundwork for more investigation into the function mechanism, this research aims to tentatively forecast the potential active components and mechanisms based on realistic constituents of JBOL in anti-IPF using biological methodologies and analysis. In the meanwhile, it also contributes to offering a point of reference for the determination of the quality control index and formulation's optimization.

Based on 118 components found in earlier studies, 34 active components were selected for this research, and the key targets were taken via the SwissTargetPrediction and TCMSP databases. 1169 IPF-related targets were obtained from OMIM, DisGeNET, and GeneCards databases, and 122 component-IPF targets were determined with intersection. We screened out the top 8 potential active ingredients by analyzing rank of degree value in the herb-compound-target network, including kaempferol, apigenin, methylnissolin, baicalein, liquiritigenin, phellopterin, peimine, cryptotanshinone.

(G)



(H)

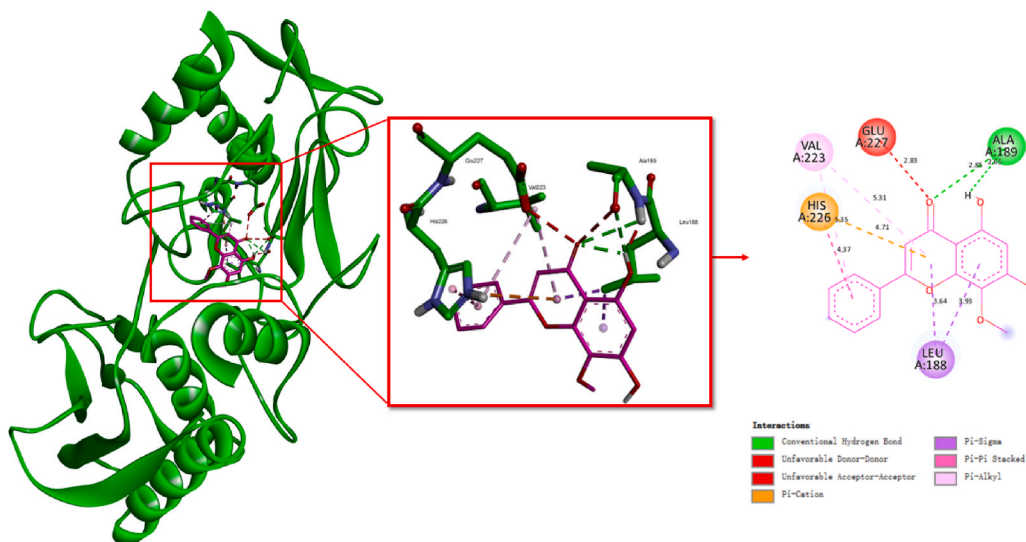


Fig. 9. (continued).

Kaempferol is one of the core ingredients existed in 5 herbs of JBOL, which exhibited a wide range of inhibition on the expression of fibrosis-related genes in transforming growth factor beta 1 (TGF- β 1) and triggered the process of EMT by reversing the expression of α -SMA and E-cadherin [43,44]. Previous *in vitro* experiments have shown that kaempferol inhibits TGF- β 1-induced fibroblast proliferation and myofibroblast differentiation by promoting the AMPK/PPAR- γ pathway, which in turn reduces excessive collagen production and the formation of scar tissue in fibrotic conditions [45]. Additional diverse pathways, like the TGF- β /Smad and Wnt/ β -catenin pathways, were implicated in the anti-fibrosis process [46]. Moreover, kaempferol could prevent the formation of inflammatory cytokines and regulate autophagy to have an anti-fibrosis effect [47]. Recent studies have shown that kaempferol influences the progression of organ fibrosis through the bone morphogenic protein 7-Smad1/5, Notch pathways, and autophagy [48], respectively.

Apigenin is a significant member of the flavonoid family with anti-fibrosis and anti-inflammatory characteristics. At the same time,

Table 4
Molecular docking results and interaction analysis for identified compounds.

Ligands Compounds	Receptor Protein	PDB ID	Hydrogenbonds	Hydrophobic interaction	E. kcal·mol ⁻¹
peimine	MTOR	4DRI	TYR-57, ARG-73	TRP-2102, TRY-2105, PHE-77, ILE-87, VAL-86, PHE-2039, PHE-2108	-11.1
cryptotanshinone	AKT1	4EJN	SER-205	LYS-268, LEU-264, TYR-272, VAL-270	-11.0
cryptotanshinone	MTOR	4DRI	SER-2035	PHE-77, PHE-2039	-10.4
apigenin	MMP9	4WZV	ALA-189	VAL-223	-10.4
kaempferol			ALA-189, GLU-227	VAL-223	-10.2
baicalein			LEU-188, ALA-189, MET-247, PRO-246	VAL-223	-10.1
liquiritigenin			ALA-189, TYR-248	VAL-223, LEU-188	-10.0
wogonin			ALA-189	VAL-223	-9.7

the exact mechanism of apigenin in inhibiting lung fibrosis and inflammation has not yet been articulated. It is involved in *Salvia miltiorrhiza* Bge; *Lonicera japonica* Thunb; *Scutellaria baicalensis* Georgi; *Codonopsis pilosula* (Franch.) Nannf in JBOL. Phosphorylated p65 levels were downregulated by apigenin, which also reduced the expression of pro-inflammatory cytokines such as caspase-3, interleukin-1 β (IL-1 β), TNF- α and TGF- β that were motivated by lipopolysaccharide (LPS) [49]. Numerous investigations have demonstrated that oxidative stress plays a major role in the progression of lung fibrosis. TGF- β , a powerful fibrosis promoter, was produced in a condition of high oxidation. Apigenin can decrease TGF- β expression in a concentration-dependent way and lessen the accumulation of collagen [50]. In short, it can prevent lung cells from experiencing oxidative stress and fibrosis cytokines [51]. Yet, further experimental validation is required to confirm the active mechanism of apigenin due to its low levels of solubility *in vitro* and bioavailability *in vivo*. Zhang J. et al. [52] looked examined the utilization of apigenin loaded in a biodegradable carrier (apigenin-NP) to treat pulmonary fibrosis and found that it could dose-dependently arrest cells in the G0/G1 phases.

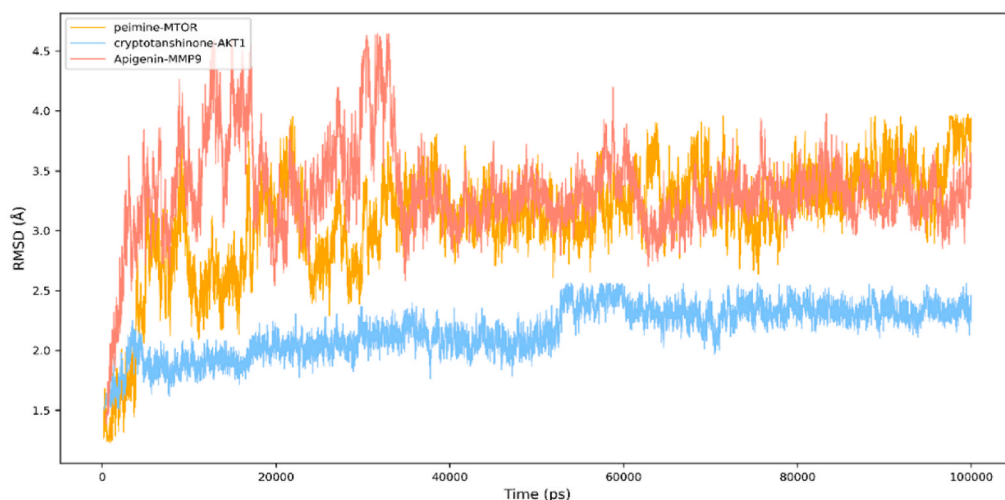
Baicalein is a common plant flavonoid with a variety of advantageous pharmacological characteristics, including anti-inflammatory, antioxidative, anti-apoptotic, pro-immunoregulatory functions. Sun [53] investigated that baicalein inhibited the differentiation of lung fibroblasts into myofibroblasts via downregulating the levels of Col1a1 and CTGF. In addition, baicalein significantly improved the proliferation and activation of NIH/3T3 by alleviating TGF β 1-induced type I collagen [54]. EGFR and AKT1 are indispensable targets for anti-IPF, while peimine could suppress the phosphorylation of EGFR, PI3K, and AKT1 to inhibit fibroblast activation [55]. Yuan et al. [56] demonstrated that baicalein arrests the development of pulmonary fibrosis by suppressing the TGF- β 1/Smad signaling pathway by downregulating the BLM-induced of lung Sirt3 expression. In addition, it also attenuated markedly mRNA levels of profibrotic senescence-associated secretory phenotype (SASP) factors, including MCP-1, PAI-1, TNF- α , MMP-10 and MMP-12 to relieve the senescence of lung fibroblasts.

Major tanshinone derived from *Salvia miltiorrhiza* Bge is identified as cryptotanshinone. According to recent research, cryptotanshinone inhibits the expression of COL1A1 and α -SMA, which provides the effects of anti-inflammatory, anti-angiogenesis, and anti-lymphangiogenesis in addition to preventing atherosclerosis and Alzheimer's disease [57,58], but also exerts multiple effects on anti-inflammatory, anti-angiogenesis, and anti-lymphangiogenesis through inhibiting the expression of α -SMA, collagen-I And the phosphorylation level of Stat3 also participate in anti-IPF [59]. To put it briefly, the aforementioned components are speculated to be the material basis of IPF.

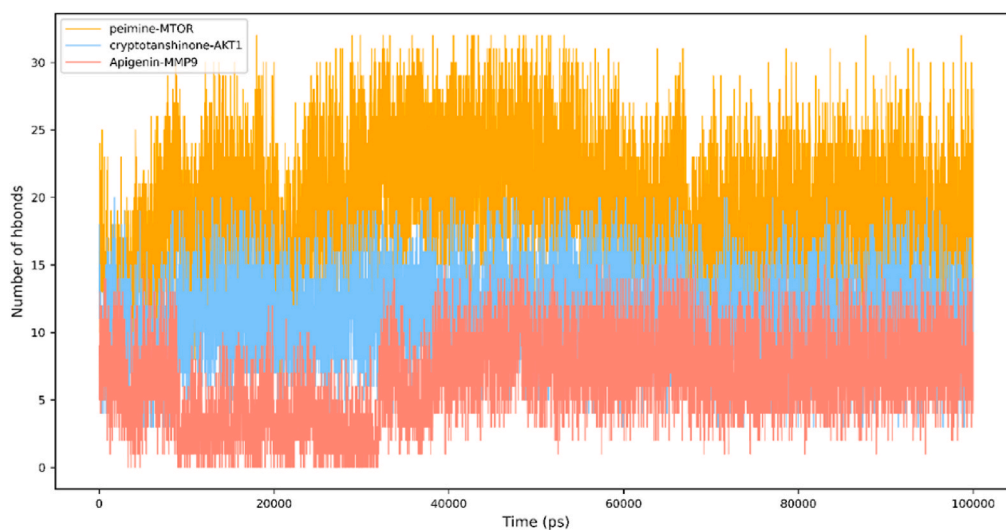
The above-mentioned studies stated that screened ingredients are closely linked with JBOL in anti-IPF. Additionally, three core components were found in *Salvia miltiorrhiza* Bge and *Astragalus membranaceus* (Fisch.) Bge, and two key components involved in *Scutellaria baicalensis* Georgi, *Lonicera japonica* Thunb, and *Glycyrrhiza uralensis* Fisch, respectively. The herb-component-target network predicts that *Astragalus membranaceus* (Fisch.) Bge and *Salvia miltiorrhiza* Bge are essential groups in JBOL and correspond to the IPF therapeutics in TCM, which followed the principles of tonifying the spleen to nourish qi and promoting blood circulation to remove blood stasis. Thus, we anticipate that the network conclusion will serve as a guide for JBOL compatibility and dosage optimization.

We performed GO and KEGG enrichment analysis to investigate the mechanism of JBOL in the treatment of IPF. Numerous biological processes, including as protein phosphorylation, signal transduction, drug reaction, inflammation, and apoptosis, were identified by GO functional analysis as being connected to the effects of JBOL in anti-IPF. Cell senescence, inflammatory response, autophagy, and immune-related pathways, which focused on the AGE-RAGE, PI3K-Akt signaling pathway, and EGFR tyrosine kinase inhibitor resistance were among the enriched targets.

Based on accumulating data, the EGFR-ligand system was crucial in the irreversible lung tissue scarring. In the meantime, the EGFR receptors and ligands were found to be overexpressed in IPF lungs [60]. It has already been demonstrated that the stimulation of fibroblasts with TGF- β 1 elevates the expression of various EGFR ligands, such as AREG, EREG, and HB-EGF, which in turn increases cell proliferation and the expression of profibrotic genes. These effects were reversed by the treatment of TGF- β 1-stimulated fibroblasts with AREG siRNA or EGFR inhibitors [61]. Moreover, several reviews indicate that the EGFR signaling cascade is upregulated in lung fibroblasts from patients with IPF [62]. The EGFR pathway promotes fibrosis by phosphorylating EGFR, which in turn stimulates a number of downstream signaling pathways, such as PIK3/Akt pathway, PLC pathway, STAT pathway, and MAPK pathway [63]. Previous research has demonstrated that the activity of EGFR in pulmonary fibrosis can be restricted through decreasing the expression of TGF and VEGF/PDGF/FGF1 receptors [64], which in turn decreases collagen synthesis and ECM deposition [65], and inhibiting



(A)



(B)

Fig. 10. Molecular dynamics simulation of peimine-MTOR, cryptotanshinone-AKT1, and apigenin-MMP9. (A) RMSD values extracted from the protein-ligand docked complexes. (B) H bond formation among peimine-MTOR, cryptotanshinone-AKT1, and apigenin-MMP9.

fibroblast proliferation.

Abnormal activation of EMT in IPF is associated with accelerated aging, which is the key to changes in wound healing [66]. The advanced glycation end-products (AGEs) have been proposed as markers of oxidative stress and aging. AGEs were proven to postpone the wound healing of epithelial cells and TGF- β 1 synthesis *in vitro* studies, and their ligand RAGEs decrease led to AGEs accumulation. All of these findings indicated that the formation and progression of IPF is caused by an imbalance between AGEs and RAGEs [67], which are correlating with the upward regulation of the AGEs-RAGEs pathway.

The PI3K/AKT signaling pathway has been significant in the intracellular regulation of cell growth, proliferation, autophagy, metabolism, and apoptosis, and it has been identified as a hotspot route in IPF [68,69], which play an important role of cellular proliferative and migration [70], cell adhesion [71]. The activation of the PI3K/AKT pathway accelerates the overexpression of α -SMA and TGF- β leading to the formation of pulmonary fibrosis [72]. In addition, it promotes pulmonary fibrosis by upregulating its downstream cytokines including mTOR and HIF-1 α , to regulate inflammatory immune response, induces EMT and ECM deposition

[73,74]. In addition to regulating the biological processes associated with IPF alone, the pathophysiology of IPF involves a range of interaction and crosstalk with signaling pathways, such as TGF, VEGF, WNT, mTOR, Jun N-terminal kinase, CTGF, Hedgehog, and Notch pathway [75]. Recent studies suggest that the suppression of PI3K/Akt signaling pathway induces the down-regulation of HIF-1 α and VEGF expression in lung tissue, which in turn interfere with angiogenesis and the IPF process [76]. It is necessary to confirm our hypothesis that these pathways play an essential part in the JBOL therapy mechanism in IPF.

To explore the potential molecular mechanism of JBOL in the treatment of IPF and verify the prediction results of network pharmacology, molecular docking studies, and molecular dynamic simulation were performed with core bioactive components and targets based on the outcome of the herb-active ingredient-target network and PPI network. The results of docking suggested that the components exhibited a satisfactory affinity with the key target proteins. These compounds and targets might contribute to the therapeutic effects of JBOL in IPF. Peimine-MTOR is among the compounds with the lowest binding affinities groups.

To identify the active components and putative signaling pathways in this study, we first performed data mining analysis based on the actual measurement of 118 components and merged it with the quantitative analysis of chemical components in JBOL, and the outcomes of the bioinformatics analysis were more rational. However, it should be pointed out that there are still some limitations in this research. As we all know, there are large discrimination of effects for the content and efficacy of active ingredients with different processing specifications and combinations [77]. For example, *Pinellia ternata* (Thunb.) Breit has some other artillery products but is not distinguished in SwissTargetPrediction and other traditional Chinese medicine information databases. Consequently, it is essential to screen accurately for each artillery drug via scientific verification. On the other hand, the accuracy and timeliness of the chemical library need to be updated, such as the amount of evidence for toxicological mechanisms is insufficient, which may lead to biases in the analysis results. Our research findings will be further validated in pharmacodynamic and molecular biology experiment in the following time.

5. Conclusion

In this study, we firstly forecasted an investigation of main active ingredients and prospective mechanisms in JBOL for the therapy of IPF, which utilizing network pharmacology, molecular docking, and molecular dynamic modeling, etc. Effect mechanism of JBOL in anti-IPF was concerned with decreasing autophagy, inflammatory, immunological response, and cell senescence through AGE-RAGE signaling pathway, EGFR signaling pathway, PI3K-Ak signaling pathway, and etc. In summary, we reviewed how JBOL exerted its therapeutic effects on anti-IPF through multi-target and multi-pathway in accordance with the core ingredients and signaling pathways predicted. Bioinformatics techniques were used to investigate the potential mechanism, providing the theoretical foundation for experimental research. The study has indicated where additional research should be performed in order to confirm the quality indicators and optimize the preparation technology. Numerous studies indicate that machine learning has been increasingly popular in recent years and has applications in a variety of fields, including biology, medicine, and healthcare [78,79]. This inspires us to combine this strategy with experiments to obtain additional verification. From a clinical application standpoint, only few research has verified that TCM compound preparation is feasible to enhance the clinically therapeutic effect of IPF, JBOL has enhanced the efficacy of IPF treatment and raised patient acceptance by decreasing adverse events. Based on extensive studies investigating, the future research should focus on the clinical applications, including determining optimal dosages, conducting clinical trials to explore the absorption, distribution, metabolism and elimination in the human body, as well as the safety and efficacy in the treatment of IPF. With the advantages of IPF treatment in multi-target and multi-pathway, JBOL, a novel TCM preparation, present a promising frontier in IPF therapy, and we supposed that conventional therapy assisted the application of phytopharmaceuticals would provide an option for reducing IPF symptoms, which could be a supplementary and alternative therapy.

CRedit authorship contribution statement

Xinru Han: Data curation, Writing – original draft. **Aijun Zhang:** Writing – review & editing. **Zhaoqing Meng:** Resources, Supervision. **Qian Wang:** Software, Validation. **Song Liu:** Data curation, Visualization. **Yunjia Wang:** Software. **Jiaxin Tan:** Validation. **Lubo Guo:** Conceptualization, Methodology, Software. **Feng Li:** Methodology, Project administration, Supervision.

Declaration of competing interest

The authors declare that they have no known competing financial interests or personal relationships that could have appeared to influence the work reported in this paper.

Acknowledgments

This work was supported by National Major Scientific and Technological Special Project for National Key Research and Development Program of China (2022YFC3501705), Natural Science Foundation of Shandong Province of China (ZR2023MH335).

Appendix

Component abbreviation	Molecule ID
A	MOL000114
B1	MOL000414
B2	MOL000422
C1	MOL000417
C2	MOL000392
D	MOL001780
E	MOL000008
F	MOL000040
G	MOL001942
H	MOL000105
I	MOL010870
J1	MOL000173
J2	MOL002714
K	MOL002929
BSS1	MOL001953
BSS2	MOL002644
C1	MOL000417
C2	MOL000392
CBM1	MOL004451
CBM2	MOL009582
CBM3	MOL004445
CX1	61361(PubChemid)
DanS1	11425923(PubChemid)
DanS2	MOL000041
DanS3	MOL007154
DanS4	MOL007088
DanS5	MOL007157
DG1	MOL003875
GC1	MOL001789
GC2	MOL001792
HQ1	14077830(PubChemid)
HQ2	MOL000390
HQ3	101679160
HQIN1	MOL002919
HQIN2	MOL002928
LQ1	MOL003330

References

- [1] L. Richeldi, H.R. Collard, M.G. Jones, Idiopathic pulmonary fibrosis, *Lancet* 389 (10082) (May 13, 2017) 1941–1952, [https://doi.org/10.1016/S0140-6736\(17\)30866-8](https://doi.org/10.1016/S0140-6736(17)30866-8). Lancet Publishing Group.
- [2] G. Raghu, S.Y. Chen, W.S. Yeh, et al., Idiopathic pulmonary fibrosis in US Medicare beneficiaries aged 65 years and older: incidence, prevalence, and survival, 2001–11 [published correction appears in *Lancet Respir Med.* 2014 Jul;2(7): e12], *Lancet Respir. Med.* 2 (7) (2014) 566–572, [https://doi.org/10.1016/S2213-2600\(14\)70101-8](https://doi.org/10.1016/S2213-2600(14)70101-8).
- [3] P. Spagnolo, J.A. Kropski, M.G. Jones, et al., Idiopathic pulmonary fibrosis: disease mechanisms and drug development, *Pharmacol. Ther.* 222 (2021) 107798, <https://doi.org/10.1016/j.pharmthera.2020.107798>.
- [4] C.J. Reynolds, M.F. Del Greco, R.J. Allen, et al., The causal relationship between gastro-oesophageal reflux disease and idiopathic pulmonary fibrosis: a bidirectional two-sample Mendelian randomisation study, *Eur. Respir. J.* 61 (5) (2023) 2201585, <https://doi.org/10.1183/13993003.01585-2022>. Published 2023 May 25.
- [5] G. Raghu, M. Remy-Jardin, J.L. Myers, et al., Diagnosis of idiopathic pulmonary fibrosis. An official ATS/ERS/JRS/ALAT clinical practice guideline, *Am. J. Respir. Crit. Care Med.* 198 (5) (2018) e44–e68, <https://doi.org/10.1164/rccm.201807-1255ST>.
- [6] L. Richeldi, R.M. du Bois, G. Raghu, et al., Efficacy and safety of nintedanib in idiopathic pulmonary fibrosis, *N. Engl. J. Med.* 370 (22) (2014) 2071–2082, <https://doi.org/10.1056/NEJMoa1402584> [published correction appears in *N Engl J Med.* 2015 Aug 20;373(8):782].
- [7] S.M. Ruwanpura, B.J. Thomas, P.G. Bardini, Pirfenidone: molecular mechanisms and potential clinical applications in lung disease, *Am. J. Respir. Cell Mol. Biol.* 62 (4) (2020) 413–422, <https://doi.org/10.1165/rcmb.2019-0328TR>.
- [8] A. Tepede, D. Yogaratnam, Nintedanib for idiopathic pulmonary fibrosis, *J. Pharm. Pract.* 32 (2) (2019) 199–206, <https://doi.org/10.1177/0897190017735242>.
- [9] P.M. George, C.M. Patterson, A.K. Reed, M. Thillai, Lung transplantation for idiopathic pulmonary fibrosis, *Lancet Respir. Med.* 7 (3) (2019) 271–282, [https://doi.org/10.1016/S2213-2600\(18\)30502-2](https://doi.org/10.1016/S2213-2600(18)30502-2).
- [10] P.M. George, A.U. Wells, R.G. Jenkins, Pulmonary fibrosis and COVID-19: the potential role for antifibrotic therapy, *Lancet Respir. Med.* 8 (8) (2020) 807–815, [https://doi.org/10.1016/S2213-2600\(20\)30225-3](https://doi.org/10.1016/S2213-2600(20)30225-3).
- [11] C. Nogales, Z.M. Mamdouh, M. List, C. Kiel, A.I. Casas, H.H.H.W. Schmidt, Network pharmacology: curing causal mechanisms instead of treating symptoms, *Trends Pharmacol. Sci.* 43 (2) (2022) 136–150, <https://doi.org/10.1016/j.tips.2021.11.004>.
- [12] S. Li, B. Zhang, N. Zhang, Network target for screening synergistic drug combinations with application to traditional Chinese medicine, *BMC Syst. Biol.* 5 (Suppl 1) (2011) S10, <https://doi.org/10.1186/1752-0509-5-S1-S10>. Published 2011 Jun 20.
- [13] L. Zhao, H. Zhang, N. Li, et al., Network pharmacology, a promising approach to reveal the pharmacology mechanism of Chinese medicine formula, *J. Ethnopharmacol.* 309 (2023) 116306, <https://doi.org/10.1016/j.jep.2023.116306>.
- [14] X., W. D., J.M.U. Zhang, Therapeutic effect and mechanism of Fei Tong oral liquid on the acute lung injury in rats, *Shandong Med. J.* 53 (2013) 8–10.

- [15] X., J. M. U., W.-C. Y. U., L. C. C., and L. Y. Y. Zhang, "Effect of Feitongkoufuye treating pulmonary interstitial fibrosis on neutrophil elastase," *J. Shandong Univ. Sci.* 50, 24–28.
- [16] P. Salaria, M.A. Reddy, Network pharmacology approach to identify the calotropis phytoconstituents' potential epileptic targets and evaluation of molecular docking, MD simulation, and MM-PBSA performance, *Chem. Biodivers.* 21 (5) (2024) e202400255, <https://doi.org/10.1002/cbdv.202400255>.
- [17] A. Daina, O. Michielin, V. Zoete, SwissADME: a free web tool to evaluate pharmacokinetics, drug-likeness and medicinal chemistry friendliness of small molecules, *Sci. Rep.* 7 (2017) 42717, <https://doi.org/10.1038/srep42717>. Published 2017 Mar 3.
- [18] J. Ru, P. Li, J. Wang, et al., TCMSP: a database of systems pharmacology for drug discovery from herbal medicines, *J. Cheminf.* 6 (2014) 13, <https://doi.org/10.1186/1758-2946-6-13>. Published 2014 Apr 16.
- [19] UniProt Consortium, UniProt: the universal protein knowledgebase in 2023, *Nucleic Acids Res.* 51 (D1) (2023) D523–D531, <https://doi.org/10.1093/nar/gkac1052>.
- [20] J.S. Amberger, C.A. Bocchini, F. Schiettecatte, A.F. Scott, A. Hamosh, OMIM.org: online Mendelian Inheritance in Man (OMIM®), an online catalog of human genes and genetic disorders, *Nucleic Acids Res.* 43 (Database issue) (2015) D789–D798, <https://doi.org/10.1093/nar/gku1205>.
- [21] J. Piñero, J.M. Ramírez-Anguita, J. Saich-Pitarch, et al., The DisGeNET knowledge platform for disease genomics: 2019 update, *Nucleic Acids Res.* 48 (D1) (2020) D845–D855, <https://doi.org/10.1093/nar/gkz1021>.
- [22] S. Pan, B. Hu, J. Sun, et al., Identification of cross-talk pathways and ferroptosis-related genes in periodontitis and type 2 diabetes mellitus by bioinformatics analysis and experimental validation, *Front. Immunol.* 13 (2022) 1015491, <https://doi.org/10.3389/fimmu.2022.1015491>. Published 2022 Sep. 29.
- [23] D. Szklarczyk, R. Kirsch, M. Koutrouli, et al., The STRING database in 2023: protein-protein association networks and functional enrichment analyses for any sequenced genome of interest, *Nucleic Acids Res.* 51 (D1) (2023) D638–D646, <https://doi.org/10.1093/nar/gkac1000>.
- [24] H. Bashiri, H. Rahmani, V. Bashiri, D. Módos, A. Bender, EMDIP: an entropy measure to discover important proteins in PPI networks, *Comput. Biol. Med.* 120 (2020) 103740, <https://doi.org/10.1016/j.compbiomed.2020.103740>.
- [25] B.J. O'Roak, L. Vives, W. Fu, et al., Multiplex targeted sequencing identifies recurrently mutated genes in autism spectrum disorders, *Science* 338 (6114) (2012) 1619–1622, <https://doi.org/10.1126/science.1227764>.
- [26] The Gene Ontology Consortium, The gene Ontology resource: 20 years and still GOing strong, *Nucleic Acids Res.* 47 (D1) (2019) D330–D338, <https://doi.org/10.1093/nar/gky1055>.
- [27] M. Kanehisa, M. Furumichi, M. Tanabe, Y. Sato, K. Morishima, KEGG: new perspectives on genomes, pathways, diseases and drugs, *Nucleic Acids Res.* 45 (D1) (2017) D353–D361, <https://doi.org/10.1093/nar/gkw1092>.
- [28] Y. Zhou, B. Zhou, L. Pache, et al., Metascape provides a biologist-oriented resource for the analysis of systems-level datasets, *Nat. Commun.* 10 (1) (2019) 1523, <https://doi.org/10.1038/s41467-019-09234-6>. Published 2019 Apr 3.
- [29] M. Kanehisa, M. Furumichi, Y. Sato, M. Kawashima, M. Ishiguro-Watanabe, KEGG for taxonomy-based analysis of pathways and genomes, *Nucleic Acids Res.* 51 (D1) (2023) D587–D592, <https://doi.org/10.1093/nar/gkac963>.
- [30] J. Reimand, R. Isserlin, V. Voisin, et al., Pathway enrichment analysis and visualization of omics data using g: Profiler, GSEA, Cytoscape and EnrichmentMap, *Nat. Protoc.* 14 (2) (2019) 482–517, <https://doi.org/10.1038/s41596-018-0103-9>.
- [31] K. Crampon, A. Giorkallos, M. Deldossi, S. Baud, L.A. Steffanel, Machine-learning methods for ligand-protein molecular docking, *Drug Discov. Today* 27 (1) (2022) 151–164, <https://doi.org/10.1016/j.drudis.2021.09.007>.
- [32] J. Eberhardt, D. Santos-Martins, A.F. Tillack, S. Forli, AutoDock Vina 1.2.0: new docking methods, expanded force field, and Python bindings, *J. Chem. Inf. Model.* 61 (8) (2021) 3891–3898, <https://doi.org/10.1021/acs.jcim.1c00203>.
- [33] S.K. Burley, C. Bhikadiya, C. Bi, et al., RCSB Protein Data Bank: Tools for visualizing and understanding biological macromolecules in 3D, *Protein Sci.* 31 (12) (2022) e4482, <https://doi.org/10.1002/pro.4482>.
- [34] T. Gaillard, Evaluation of AutoDock and AutoDock Vina on the CASF-2013 benchmark, *J. Chem. Inf. Model.* 58 (8) (2018) 1697–1706, <https://doi.org/10.1021/acs.jcim.8b00312>.
- [35] Chuan Tian, et al., ff19SB: amino-acid-specific protein backbone parameters trained against quantum mechanics energy surfaces in solution, *J. Chem. Theor. Comput.* 16 (1) (2019) 528–552.
- [36] K.Y. Hsin, S. Ghosh, H. Kitano, Combining machine learning systems and multiple docking simulation packages to improve docking prediction reliability for network pharmacology, *PLoS One* 8 (12) (2013) e83922, <https://doi.org/10.1371/journal.pone.0083922>. Published 2013 Dec 31.
- [37] T.H.G. Phan, P. Paliogiannis, G.K. Nasrallah, et al., Emerging cellular and molecular determinants of idiopathic pulmonary fibrosis, *Cell. Mol. Life Sci.* 78 (5) (2021) 2031–2057, <https://doi.org/10.1007/s00018-020-03693-7>.
- [38] B.J. Moss, S.W. Ryter, I.O. Rosas, Pathogenic mechanisms underlying idiopathic pulmonary fibrosis, *Annu. Rev. Pathol.* 17 (2022) 515–546, <https://doi.org/10.1146/annurev-pathol-042320-030240>.
- [39] E.C. Oates, K.J. Jones, S. Donkervoort, et al., Congenital Titinopathy: comprehensive characterization and pathogenic insights, *Ann. Neurol.* 83 (6) (2018) 1105–1124, <https://doi.org/10.1002/ana.25241>.
- [40] A.H. El-Sherief, C.T. Lau, C.C. Wu, R.L. Drake, G.F. Abbott, T.W. Rice, International association for the study of lung cancer (IASLC) lymph node map: radiologic review with CT illustration, *Radiographics* 34 (6) (2014) 1680–1691, <https://doi.org/10.1148/rg.346130097>.
- [41] C. Zhang, Q. Cui, J. Tian, P. Wang, L. Hou, T. Gong, et al., Effect of Jinbei oral liquid on bleomycin-induced pulmonary fibrosis in rats, *Pharmacol. Clin. Chin. Materia Medica* 34 (2018) 146–150.
- [42] A. Zhang, Y. Zou, Q. Xu, et al., Investigation of the pharmacological effect and mechanism of Jinbei oral liquid in the treatment of idiopathic pulmonary fibrosis using network pharmacology and experimental validation, *Front. Pharmacol.* 13 (2022) 919388, <https://doi.org/10.3389/fphar.2022.919388>. Published 2022 Jun 15.
- [43] D. Yu, Y. Xiang, T. Gou, et al., New therapeutic approaches against pulmonary fibrosis, *Bioorg. Chem.* 138 (2023) 106592, <https://doi.org/10.1016/j.bioorg.2023.106592>.
- [44] Y. Guan, D. Quan, K. Chen, et al., Kaempferol inhibits renal fibrosis by suppression of the sonic hedgehog signaling pathway, *Phytomedicine* 108 (2023) 154246, <https://doi.org/10.1016/j.phymed.2022.154246>.
- [45] L. Yan, M.Y. Jiang, X.S. Fan, Research into the anti-pulmonary fibrosis mechanism of Renshen Pingfei formula based on network pharmacology, metabolomics, and verification of AMPK/PPAR- γ pathway of active ingredients, *J. Ethnopharmacol.* 317 (2023) 116773, <https://doi.org/10.1016/j.jep.2023.116773>.
- [46] A. Sharma, S. Waikar, Flavonoids for treating pulmonary fibrosis: present status and future prospects, *Phytother. Res.* 10 (2024 Jul), <https://doi.org/10.1002/ptr.8285>. Epub ahead of print. PMID: 38986681.
- [47] J.H. Gong, I.H. Cho, D. Shin, S.Y. Han, S.H. Park, Y.H. Kang, Inhibition of airway epithelial-to-mesenchymal transition and fibrosis by kaempferol in endotoxin-induced epithelial cells and ovalbumin-sensitized mice, *Lab. Invest.* 94 (3) (2014) 297–308, <https://doi.org/10.1038/labinvest.2013.137>.
- [48] M. Jiang, C. Huang, Q. Wu, Y. Su, X. Wang, Z. Xuan, Y. Wang, F. Xu, C. Ge, Sini San ameliorates CCl₄-induced liver fibrosis in mice by inhibiting AKT-mediated hepatocyte apoptosis, *J. Ethnopharmacol.* 303 (2023) 115965, <https://doi.org/10.1016/j.jep.2022.115965>.
- [49] C.H. Lin, C.H. Shih, B.C. Chen, Thrombin-induced IL-8/CXCL8 release is mediated by CK2, MSK1, and NF- κ B pathways in human lung epithelial cells, *Eur. J. Pharmacol.* 767 (2015) 135–143, <https://doi.org/10.1016/j.ejphar.2015.10.018>.
- [50] L. Chen, W. Zhao, Apigenin protects against bleomycin-induced lung fibrosis in rats, *Exp. Ther. Med.* 11 (1) (2016) 230–234, <https://doi.org/10.3892/etm.2015.2885>.
- [51] D.A. Sawatzky, D.A. Willoughby, P.R. Colville-Nash, A.G. Rossi, The involvement of the apoptosis-modulating proteins ERK 1/2, Bcl-xL and Bax in the resolution of acute inflammation in vivo, *Am. J. Pathol.* 168 (1) (2006) 33–41, <https://doi.org/10.2353/ajpath.2006.050058>.
- [52] J. Zhang, L. Chao, X. Liu, et al., The potential application of strategic released apigenin from polymeric carrier in pulmonary fibrosis, *Exp. Lung Res.* 43 (9–10) (2017) 359–369, <https://doi.org/10.1080/01902148.2017.1380086>.
- [53] X. Sun, X. Cui, X. Chen, X. Jiang, Baicalein alleviated TGF β 1-induced type I collagen production in lung fibroblasts via downregulation of connective tissue growth factor, *Biomed. Pharmacother.* 131 (2020) 110744, <https://doi.org/10.1016/j.biopha.2020.110744>.

- [54] N.N.T. Sisin, N.F.C. Mat, R.A. Rashid, et al., Natural baicalein-rich fraction as radiosensitizer in combination with bismuth oxide nanoparticles and cisplatin for clinical radiotherapy, *Int. J. Nanomed.* 17 (2022) 3853–3874, <https://doi.org/10.2147/IJN.S370478>. Published 2022 Sep. 2.
- [55] D. Shao, X. Liu, J. Wu, et al., Identification of the active compounds and functional mechanisms of Jinshui Huanxian formula in pulmonary fibrosis by integrating serum pharmacokinetics with network pharmacology, *Phytomedicine* 102 (2022) 154177, <https://doi.org/10.1016/j.phymed.2022.154177>.
- [56] Y. Ji-Hong, M. Yu, Y. Ling-Hong, et al., Baicalein attenuates bleomycin-induced lung fibroblast senescence and lung fibrosis through restoration of Sirt3 expression, *Pharm. Biol.* 61 (1) (2023) 288–297, <https://doi.org/10.1080/13880209.2022.2160767>.
- [57] D. Hao, W. Danbin, G. Maojuan, et al., Ethanol extracts of Danlou tablet attenuate atherosclerosis via inhibiting inflammation and promoting lipid effluent, *Pharmacol. Res.* 146 (2019) 104306, <https://doi.org/10.1016/j.phrs.2019.104306>.
- [58] F. Maione, M. Piccolo, S. De Vita, et al., Down regulation of pro-inflammatory pathways by tanshinone IIA and cryptotanshinone in a non-genetic mouse model of Alzheimer's disease, *Pharmacol. Res.* 129 (2018) 482–490, <https://doi.org/10.1016/j.phrs.2017.11.018>.
- [59] Q. Zhang, C. Gan, H. Liu, et al., Cryptotanshinone reverses the epithelial-mesenchymal transformation process and attenuates bleomycin-induced pulmonary fibrosis, *Phytother. Res.* 34 (10) (2020) 2685–2696, <https://doi.org/10.1002/ptr.6699>.
- [60] H.T. Hsu, C.C. Yu, Y.H. Lee, J.C. Chan, C.Y. Chu, Association between dermatologic adverse events and quality of life in lung cancer patients treated with epidermal growth factor receptor-tyrosine kinase inhibitors, *Support. Care Cancer* 30 (11) (2022) 9211–9219, <https://doi.org/10.1007/s00520-022-07347-1>.
- [61] F. Schramm, L. Schaefer, M. Wygrecka, EGFR signaling in lung fibrosis, *Cells* 11 (6) (2022) 986, <https://doi.org/10.3390/cells11060986>. Published 2022 Mar 14.
- [62] I.T. Stancil, J.E. Michalski, D. Davis-Hall, et al., Pulmonary fibrosis distal airway epithelia are dynamically and structurally dysfunctional, *Nat. Commun.* 12 (1) (2021) 4566, <https://doi.org/10.1038/s41467-021-24853-8>. Published 2021 Jul 27.
- [63] X. Tao, H. Liu, J. Xia, et al., Processed product (Pinelliae Rhizoma Praeparatum) of *Pinellia ternata* (Thunb.) Breit. Alleviates the allergic airway inflammation of cold phlegm via regulation of PKC/EGFR/MAPK/PI3K-AKT signaling pathway, *J. Ethnopharmacol.* 295 (2022) 115449, <https://doi.org/10.1016/j.jep.2022.115449>.
- [64] H.V. Woodcock, P.L. Molyneaux, T.M. Maher, Reducing lung function decline in patients with idiopathic pulmonary fibrosis: potential of nintedanib, *Drug Des. Dev. Ther.* 7 (2013) 503–510, <https://doi.org/10.2147/DDDT.S38833>. Published 2013 Jun 19.
- [65] I.D. Odell, H. Steach, S.B. Gauld, et al., Epiregulin is a dendritic cell-derived EGFR ligand that maintains skin and lung fibrosis, *Sci Immunol* 7 (78) (2022) eabq6691, <https://doi.org/10.1126/sciimmunol.Abq6691>.
- [66] P.P. Ogger, G.J. Albers, R.J. Hewitt, et al., Itaconate controls the severity of pulmonary fibrosis, *Sci Immunol* 5 (52) (2020) eabc1884, <https://doi.org/10.1126/sciimmunol.abcl1884>.
- [67] C. Machahua, A. Montes-Worboys, R. Llatjos, et al., Increased AGE-RAGE ratio in idiopathic pulmonary fibrosis, *Respir. Res.* 17 (1) (2016) 144, <https://doi.org/10.1186/s12931-016-0460-2>. Published 2016 Nov 5.
- [68] M.S. Khan, S. Dwivedi, M. Priyadarshini, et al., Ribosylation of bovine serum albumin induces ROS accumulation and cell death in cancer line (MCF-7), *Eur. Biophys. J.* 42 (11–12) (2013) 811–818, <https://doi.org/10.1007/s00249-013-0929-6>.
- [69] H. Gong, X. Lyu, Y. Liu, et al., Eupatilin inhibits pulmonary fibrosis by activating Sestrin2/PI3K/Akt/mTOR dependent autophagy pathway, *Life Sci.* 334 (2023) 122218, <https://doi.org/10.1016/j.lfs.2023.122218>.
- [70] K. Chen, Y. Li, X. Zhang, R. Ullah, J. Tong, Y. Shen, The role of the PI3K/AKT signaling pathway in the corneal epithelium: recent updates, *Cell Death Dis.* 13 (5) (2022) 513, <https://doi.org/10.1038/s41419-022-04963-x>. Published 2022 May 31.
- [71] C. Godoy-Parejo, C. Deng, W. Liu, G. Chen, Insulin stimulates PI3K/AKT and cell adhesion to promote the survival of individualized human embryonic stem cells, *Stem Cell.* 37 (8) (2019) 1030–1041, <https://doi.org/10.1002/stem.3026>.
- [72] L. Fang, H. Chen, R. Kong, J. Que, Endogenous tryptophan metabolite 5-Methoxytryptophan inhibits pulmonary fibrosis by downregulating the TGF- β /SMAD3 and PI3K/AKT signaling pathway, *Life Sci.* 260 (2020) 118399, <https://doi.org/10.1016/j.lfs.2020.118399>.
- [73] L.J. Garcia-Morales, N.Y. Chen, T. Weng, et al., Altered hypoxic-adenosine Axis and metabolism in group III pulmonary hypertension, *Am. J. Respir. Cell Mol. Biol.* 54 (4) (2016) 574–583, <https://doi.org/10.1165/rcmb.2015-0145OC>.
- [74] X. Pei, F. Zheng, Y. Li, et al., Niclosamide ethanolate salt alleviates idiopathic pulmonary fibrosis by modulating the PI3K-mTORC1 pathway, *Cells* 11 (3) (2022) 346, <https://doi.org/10.3390/cells11030346>. Published 2022 Jan 20.
- [75] J. Wang, K. Hu, X. Cai, et al., Targeting PI3K/AKT signaling for treatment of idiopathic pulmonary fibrosis, *Acta Pharm. Sin.* B 12 (1) (2022) 18–32, <https://doi.org/10.1016/j.apsb.2021.07.023>.
- [76] L. C. C. A. V. L., et al., Common molecular pathways targeted by nintedanib in cancer and IPF: a bioinformatic study, *Pulm. Pharmacol. Ther.* 64 (2020) 101941, <https://doi.org/10.1016/j.pupt.2020.101941>.
- [77] J. Chen, L.F. Li, Z.Z. Lin, X.L. Cheng, F. Wei, S.C. Ma, A quality-comprehensive-evaluation-index-based model for evaluating traditional Chinese medicine quality, *Chin. Med.* 18 (1) (2023) 89, <https://doi.org/10.1186/s13020-023-00782-0>. Published 2023 Jul 28.
- [78] W. Bao, Y. Gu, B. Chen, H. Yu, Golgi_DF: golgi proteins classification with deep forest, *Front. Neurosci.* 17 (2023) 1197824, <https://doi.org/10.3389/fnins.2023.1197824>.
- [79] W. Bao, Y. Liu, B. Chen, Oral_voting_transfer: classification of oral microorganisms' function proteins with voting transfer model, *Front. Microbiol.* 14 (2024) 1277121, <https://doi.org/10.3389/fmicb.2023.1277121>.